



NAVAL POSTGRADUATE SCHOOL

MONTEREY, CALIFORNIA

THESIS

**THE USE OF COMMERCIAL REMOTE SENSING IN
PREDICTING HELICOPTER BROWNOUT CONDITIONS**

by

Christine Kay Rabaja

September 2009

Thesis Advisor:
Second Reader:

Richard C. Olsen
David M. Trask

Approval for public use; distribution is unlimited.

REPORT DOCUMENTATION PAGE			<i>Form Approved OMB No. 0704-0188</i>	
Public reporting burden for this collection of information is estimated to average 1 hour per response, including the time for reviewing instruction, searching existing data sources, gathering and maintaining the data needed, and completing and reviewing the collection of information. Send comments regarding this burden estimate or any other aspect of this collection of information, including suggestions for reducing this burden, to Washington headquarters Services, Directorate for Information Operations and Reports, 1215 Jefferson Davis Highway, Suite 1204, Arlington, VA 22202-4302, and to the Office of Management and Budget, Paperwork Reduction Project (0704-0188) Washington DC 20503.				
1. AGENCY USE ONLY (Leave blank)		2. REPORT DATE September 2009	3. REPORT TYPE AND DATES COVERED Master's Thesis	
4. TITLE AND SUBTITLE The Use of Commercial Remote Sensing Systems in Predicting Helicopter Brownout Conditions			5. FUNDING NUMBERS	
6. AUTHOR Christine Kay Rabaja				
7. PERFORMING ORGANIZATION NAME(S) AND ADDRESS(ES) Naval Postgraduate School Monterey, CA 93943-5000			8. PERFORMING ORGANIZATION REPORT NUMBER	
9. SPONSORING /MONITORING AGENCY NAME(S) AND ADDRESS(ES) N/A			10. SPONSORING/MONITORING AGENCY REPORT NUMBER	
11. SUPPLEMENTARY NOTES The views expressed in this thesis are those of the author and do not reflect the official policy or position of the Department of Defense or the U.S. Government.				
12a. DISTRIBUTION / AVAILABILITY STATEMENT Approved for public release; distribution is unlimited.			12b. DISTRIBUTION CODE	
13. ABSTRACT (maximum 200 words) Polarimetric Synthetic Aperture Radar (SAR) data from RADARSAT-2 is analyzed for detection of soils susceptible to helicopter brownout. Helicopter brownout occurs when downwash disturbs the dust and sand beneath the aircraft during takeoff, landing, and low altitude operations. Brownout may lead to pilot spatial disorientation and loss of control, causing helicopter damage or destruction, as well as personnel injury or death. The likelihood of helicopter brownout is related to soil moisture content, particle size distribution, and surface texture. This research explores the polarimetric signatures of soils, and determines if these characteristics can be used to predict areas that are susceptible to helicopter brownout. Preliminary results show that helicopter brownout regions can be predicted by means of a simple threshold.				
14. SUBJECT TERMS Radar Polarimetry, Quadrature polarimetry, Helicopter Brownout			15. NUMBER OF PAGES 91	
			16. PRICE CODE	
17. SECURITY CLASSIFICATION OF REPORT Unclassified	18. SECURITY CLASSIFICATION OF THIS PAGE Unclassified	19. SECURITY CLASSIFICATION OF ABSTRACT Unclassified	20. LIMITATION OF ABSTRACT UU	

NSN 7540-01-280-5500

Standard Form 298 (Rev. 2-89)
Prescribed by ANSI Std. Z39-18

THIS PAGE INTENTIONALLY LEFT BLANK

Approved for public release; distribution is unlimited

**THE USE OF COMMERCIAL REMOTE SENSING SYSTEMS IN PREDICTING
HELICOPTER BROWNOUT CONDITIONS**

Christine Kay Rabaja
Major, United States Marine Corps
B.S., The University of Iowa, 1996
M.B.A, Webster University, 2006

Submitted in partial fulfillment of the
requirements for the degree of

MASTER OF SCIENCE IN SPACE SYSTEMS OPERATIONS

from the

**NAVAL POSTGRADUATE SCHOOL
September 2009**

Author: Christine Kay Rabaja

Approved by: Richard C. Olsen
Thesis Advisor

David M. Trask
Second Reader

Rudolf Panholzer
Chair, Space Systems Academic Group

THIS PAGE INTENTIONALLY LEFT BLANK

ABSTRACT

Polarimetric Synthetic Aperture Radar (SAR) data from RADARSAT-2 is analyzed for detection of soils susceptible to helicopter brownout. Helicopter brownout occurs when downwash disturbs the dust and sand beneath the aircraft during takeoff, landing, and low altitude operations. Brownout may lead to pilot spatial disorientation and loss of control, causing helicopter damage or destruction, as well as personnel injury or death. The likelihood of helicopter brownout is related to soil moisture content, particle size distribution, and surface texture. This research explores the polarimetric signatures of soils, and determines if these characteristics can be used to predict areas that are susceptible to helicopter brownout. Preliminary results show that helicopter brownout regions can be predicted by means of a simple threshold.

THIS PAGE INTENTIONALLY LEFT BLANK

TABLE OF CONTENTS

I.	INTRODUCTION.....	1
A.	PURPOSE OF RESEARCH	1
B.	OBJECTIVE	1
II.	BACKGROUND	3
A.	PREVIOUS WORK IN HELICOPTER BROWNOUT	3
1.	Definition of Helicopter Brownout	3
2.	Safety Related Information.....	5
3.	Other Writings in Helicopter Brownout.....	6
B.	PHYSICAL PROPERTIES OF SOIL	7
1.	General.....	7
2.	Soil Texture and Particle Size Distribution	7
3.	Surface Roughness	12
4.	Soil Water Content and the Correlation with Dielectric Constant	14
5.	Soils, Thesis Specific	16
C.	REMOTE SENSING VIA THE ELECTROMAGNETIC SPECTRUM	16
1.	Electromagnetic Spectrum	16
2.	Imaging Radar	18
3.	Radar Backscatter	19
D.	POLARIMETRIC RADAR	20
E.	BASICS OF RADAR IMAGE INTERPRETATION AND ANALYSIS..	23
1.	Research Image Analysis System	24
2.	Preprocessing Function	24
3.	Image Transformation.....	24
4.	Image Classification and Analysis.....	26
F.	REMOTE SENSING TECHNOLOGY	28
1.	RADARSAT-2	28
2.	RADARSAT-2 Product Types	29
3.	Science and Operational Applications Research	30
III.	DESCRIPTION OF DATA COLLECTION.....	31
A.	RESEARCH AREA OF INTEREST	31
1.	Location	31
2.	Area of Interest Specifics.....	31
B.	RADARSAT-2 DATA SET	32
IV.	OBSERVATIONS AND ANALYSIS.....	33
A.	METHOD OVERVIEW.....	33
B.	PROCURE RADAR DATA SET	34
C.	GEOREFERENCE THE RADAR DATA.....	34
D.	IMAGE TRANSFORMATION.....	35
E.	IDENTIFY AREAS OF INTEREST.....	38

F.	HISTOGRAMS	38
G.	PARTITION BY DIGITAL NUMBERS	42
H.	DENSITY SLICE.....	43
I.	BROWNOUT ALGORITHM.....	46
J.	RESULTS	46
K.	IN-DEPTH ANALYSIS.....	47
V.	CONCLUSION	57
VI.	CONSIDERATIONS FOR FOLLOW-ON ACTIVITIES.....	59
A.	GENERAL RECOMMENDATIONS	59
1.	Applications	59
2.	Validation.....	59
	APPENDIX A. IDL CODES FOR INDIVIDUAL HISTOGRAMS	61
	APPENDIX B. IDL CODES FOR COMBINED HISTOGRAM	63
	APPENDIX C. IDL CODES FOR TWENTY PERCENT IMAGE.....	65
	APPENDIX D. IDL CODES FOR TEN PERCENT IMAGE	69
	LIST OF REFERENCES	71
	INITIAL DISTRIBUTION LIST	75

LIST OF FIGURES

Figure 1.	CH-53E Super Stallion Dusty Descent (From personal communication from the Naval Safety Center, 2009)	4
Figure 2.	Size Separates for <2 mm Mineral Material (From Soil Survey Manual, 2008)	8
Figure 3.	Sizes of particles of indicated diameters (d) in millimeters (From Soil Survey Manual, 2008).....	9
Figure 4.	Percentages of clay, silt, and sand in the basic textural classes (From Soil Survey Manual, 2008).....	10
Figure 5.	Effects of Wind Erosion (From Anthoni, 2000)	12
Figure 6.	The dielectric constant as a function of water content (From Olsen, 2007, p. 192)	15
Figure 7.	Illustration of an electromagnetic wave, where M is the magnetic field and E is the electric field (From “Glossary of Remote Sensing Terms,” 2005).....	17
Figure 8.	Four interactions of electromagnetic radiation (From “Photodermatology/Photobiology,” 2008)	18
Figure 9.	The microwave portion of the electromagnetic spectrum (From “Radar and Stereoscopy,” 2007)	19
Figure 10.	Radar systems create polarized EM waves (After “Glossary of Remote Sensing Terms,” 2005).....	21
Figure 11.	Illustration of how vertically polarized waves are backscattered by vertical dipoles, while horizontally polarized waves pass through the dipoles and are scattered by the ground underneath (From “Glossary of Remote Sensing Terms,” 2005).....	22
Figure 12.	Basic illustration of classification of multi-channel data sets (A) by pixel into classes within an image (B) (From “Fundamentals of Remote Sensing,” 2007).....	26
Figure 13.	Illustration of Unsupervised Classification (From “Fundamentals of Remote Sensing,” 2007)	28
Figure 14.	Artist Depiction of RADARSAT-2 Artwork © MacDonald, Dettwiler and Associates, Ltd. 2009 All Rights Reserved	29
Figure 15.	Research area of interest within Yuma Proving Ground, where the yellow box indicates the landing zone which is highly susceptible to brownout (From Google Earth, 2009).....	32
Figure 16.	Georeferenced polarimetric radar image of the area of interest within Yuma Proving Ground(the yellow box denotes the brownout landing zone...)	35
Figure 17.	Twenty percent compressed polarimetric radar image of the area of interest within Yuma Proving Ground.....	36
Figure 18.	Ten percent compressed polarimetric radar image of the area of interest within Yuma Proving Ground.....	37
Figure 19.	Illustration of the histogram using ten percent polarimetric radar data in the Horizontal transmit-Horizontal receive (HH) mode	39

Figure 20.	Illustration of the histogram using ten percent polarimetric radar data in the Vertical transmit-Vertical receive (VV) mode.....	40
Figure 21.	Illustration of the histogram using ten percent polarimetric radar data in the Vertical transmit-Horizontal receive (VH) mode	41
Figure 22.	Illustration of the histogram using ten percent polarimetric radar data in the Horizontal transmit-Horizontal receive (HH) mode (colored in blue) combined with the Vertical transmit-Vertical receive (VV) mode (colored in red)	42
Figure 23.	Grayscale of polarimetric radar image (VV polarization)	44
Figure 24.	Polarimetric radar image after Brownout Algorithm is applied	45
Figure 25.	Scatter plot comparing VV polarization to HH polarization which shows the VV thresholds (breaks at 3000, 4000, and 5000).....	48
Figure 26.	Scatter plot comparing HH polarization to HV polarization which shows the VV thresholds (breaks at 3000, 4000, and 5000).....	49
Figure 27.	Polarimetric radar image (VV polarization) after new Brownout Algorithm threshold values are applied (Landing Zone 1 denoted by blue box)	50
Figure 28.	Histogram of the red, sienna, yellow, and green regions of the brownout algorithm using the HH polarization (there is also a dark component with very low frequency and low digital number not visible on this scale)	51
Figure 29.	Mean values for each region of interest by polarization.....	52
Figure 30.	Histogram of the green region of interest for all four polarizations using the region defined by VV values greater than 5000	53
Figure 31.	Histogram of the yellow region of interest for all four polarizations using the region defined by VV values from 4000–5000.....	54
Figure 32.	Histogram of the red region of interest for all four polarizations using the region defined by VV values less than 3000	55

LIST OF TABLES

Table 1.	The Area of Interest (Latitude/Longitude) of Yuma Proving Ground.....	31
Table 2.	Threshold Values.	42
Table 3.	Updated threshold values	47

THIS PAGE INTENTIONALLY LEFT BLANK

ACKNOWLEDGMENTS

I consider myself exceedingly fortunate for having the opportunity to come to this institution. It is with much gratitude to MGen Tryon for believing that I could accomplish this goal, and to Col Goulet for his steady support.

The contribution of data from the Canadian Space Agency through the Science and Operational Applications Research for the RADARSAT-2 program (SOAR) was greatly appreciated.

Many thanks to Dr. Chris Olsen for taking me as a thesis student and for his guidance during all aspects of this work.

Thanks to Col. David Trask for agreeing to be my second reader and for his assistance.

My eternal gratitude to Angie (Puetz) Kim who was instrumental in my completing this thesis.

Lastly, my family continues to be my source of inspiration and support, and my love and thanks goes out to them: Dad, Mom, David, Doug, Rich, Dan, and Carol.

*“This paper by its very length defends itself against the risk
of being read.”*

—Winston Churchill

THIS PAGE INTENTIONALLY LEFT BLANK

I. INTRODUCTION

A. PURPOSE OF RESEARCH

The fundamental question of this thesis addresses whether helicopter brownout can be remotely predicted using polarimetric radar. The goal is to analyze soil moisture content, particle size distribution, and surface texture to determine how these different soil characteristics affect visibility on helicopter takeoff and landing operations, and whether soil characteristics create distinguishable polarimetric radar signatures. Several theses have been completed about the detection and prediction of helicopter brownout; this thesis will present the first work to yield measurements using polarimetric radar.

B. OBJECTIVE

The primary objective of this thesis is to analyze various soil characteristics and how those characteristics relate to helicopter brownout. The intensities of return of different wavelengths of Synthetic Aperture Radar (SAR) data were analyzed within various polarizations and the complex component of the return was then correlated with the soil characteristics. Synthetic Aperture Radar was compared to ground truth data gathered during previous theses. This data was analyzed to determine if a correlation exists between the various soil characteristics and the helicopter brownout conditions. This thesis contains chapters that provide a brief background on helicopter brownout, a thorough explanation of polarimetric radar, a detailed description of the data and the results of the research.

Chapter II introduces the phenomenon of helicopter brownout as well as a thorough explanation of polarimetric radar. Furthermore, this chapter provides information concerning soil characterization instrumental to this research.

Chapter III describes the data collection necessary for this research, including the remote sensing technologies.

Chapter IV provides details of observations and analyses of the polarimetric radar data. The visual and statistical analyses of the polarimetric radar data are also included.

Chapter V characterizes the conclusions drawn from the research, and Chapter VI provides suggestions for further research.

II. BACKGROUND

A. PREVIOUS WORK IN HELICOPTER BROWNOUT

1. Definition of Helicopter Brownout

Imagine a person driving past a long stretch of flat highway at dusk. It is a familiar road, so the vehicle is moving along at a comfortable speed. Suddenly, there is a flash of lightning in the rearview mirror, and as the driver realizes that he is about to be overtaken by a summer storm, he begins to slow down. As the sky darkens, the driver looks to his left through the window and he sees the heavy raindrops begin to overtake his vehicle. Slowing down even more, the driver looks forward and realizes that the downpour is so dense that he can no longer see the road ahead of him. Silently hoping that there are not any obstacles in front of him, he slowly pulls his vehicle over to the side of the road to wait for the visibility to become clear again.

Now imagine a helicopter pilot and crew are flying a Blackhawk helicopter to an unimproved and dusty landing zone. The arid climate has consumed any trace of water from the ground below, and the only signs of life for miles are the military vehicles waiting for the helicopter.

We're about 75 feet off the ground and 150 feet from the Humvees when the Blackhawk's rotors kick up dust and sand. "Call the dust," pilot Scott Brown orders over the headset to his crew chief and medic. Both are hanging out the windows, peering back at the cloud boiling up quickly behind us and calling: 'Dust at the tail wheel!' 'Dust at the cargo door!' 'Dust at the landing gear!' 'Dust at the cockpit door!' Brown gently sets the Blackhawk down in a roll-on landing as the seething cloud billows over the bird. Our own mini sandstorm is so thick and dark that we sit for 30 seconds until it settles enough for Brown to release his crew. (Sabbagh, 2006)

Just as the rain obscured the driver's vision, the pilot of the Blackhawk helicopter was unable to see through the dust in order to land safely.

Rotation of the main rotor blades of the helicopter creates lift, in turn creating the downward force of air called downwash. Consequently, "helicopter brownout" describes when downwash disturbs the dust and sand beneath the aircraft during takeoff, landing,

and low altitude operations (see Figure 1). The weight of the helicopter, the size of the rotor blades, and similar aerodynamic properties intrinsically affect the downwash; consequently, a larger, heavier helicopter will produce a more significant downwash than a smaller, lighter one. In order to understand brownout, it is important to study the characteristics of the surface material, which determine the quantity of dust and debris underneath the aircraft that is swept into the air by the resulting downwash. This circulating dirt and sand reduces flight visibility, which obscures the pilot's ability to determine outside visual references necessary to control the aircraft near the ground ("Brownout (aviation)," 2009). This dust cloud can lead to pilot spatial disorientation and loss of control, causing helicopter damage or destruction, as well as personnel injury or death.



Figure 1. CH-53E Super Stallion Dusty Descent
(From personal communication from the Naval Safety Center, 2009)

Visual obscuration due to brownout is often estimated by the helicopter pilot using a heuristic: the measurement of the diameter of the main rotor approximates the altitude at which the dust conditions can exist. In the illustration above, the main rotor diameter of United States Marine Corps CH-53E Super Stallion helicopter is 79 feet. Accordingly, these helicopter pilots generally presume brownout they will not experience brownout above 79 feet above the ground (AGL). However, active engagement in current military operations has these helicopter pilots encountering dust clouds beyond this heuristic, which increases the chances of spatial disorientation. “In fact, brownouts are probably the most significant of all military operational challenges when landing in a desert environment” (“Sandblaster program aims to reduce helicopter accidents caused by brownouts,” 2009).

No matter when the brownout conditions are encountered, even the most experienced pilots find that attempting to land is a daunting task. During a landing approach, the dust cloud begins near the tail of the helicopter, and as the pilot continues to slow the aircraft and the helicopter descends toward the ground, the dust cloud billows outward from beneath the aircraft until it surrounds the entire aircraft and conceals the pilot’s visual reference points on the ground. Without these visual cues, the pilot has no way to determine either how fast the helicopter is moving or the height above the ground. The greater the number of airborne particles, the more difficult it can be to retain ground visual cues necessary to land safely. Moreover, safely executing a landing in brownout conditions is even more difficult when considering the added effects of multiple helicopters or while using Night Vision Devices (NVDs). While manageable through extensive training, brownouts represent a serious operational challenge for rotary wing aviation.

2. Safety Related Information

In his 30 May 2007, Memorandum for Secretaries of Military Departments, the Honorable Robert Gates wrote, “We can no longer tolerate the injuries, costs, and capability losses from preventable accidents” (2007). Yet, while pilots train extensively in dusty conditions, accidents can and often do happen.

Also known as Degraded Visual Environments (DVE), brownout conditions lead to aircraft mishaps called Controlled Flight into Terrain (CFIT). The Naval Safety Center defines CFIT as a “collision with terrain, water, trees or a man-made obstacle during flight prior to planned touchdown” (2009). This definition differentiates mishaps when the helicopter pilot is actively controlling the aircraft but has become spatially disoriented after losing sight of the ground reference points from accidents that occur when the pilot has lost control of the aircraft due to some mechanical problem. Examples of CFIT due to DVE are drifting sideways into another aircraft; an unintentional turn that causes the tail rotor to hit a tree; and rolling the aircraft away from a level attitude and striking the main rotors against a building. Practiced published procedures and extensive training mitigate of the tremendous risk associated with brownout; however, it is the opinion of this author that these types of mishaps can be prevented if brownout conditions are circumvented.

“Operations in Afghanistan and Iraq have once again thrown combat helicopters into the spotlight, proving that they are essential tools for supply, re-arming, troop movements, top cover, convoy escort and morale-boosting mail deliveries, especially in difficult and dangerous locations” (Skinner, 2008). However, the number of brownout-related accidents has more than doubled since operations began in these regions (Jennings, 2008). For example, the United States Army suffered 41 brownout incidents between 2002 and 2005. This is clearly illustrated by the increase of brownout-related accidents from 8.7 percent before the invasion of Iraq to 17.6 percent during it (Jennings, 2008). “Brownouts are a major factor attributed to a number of helicopter losses, and tactics and technology are being developed to alleviate the issue” (Skinner, 2008).

3. Other Writings in Helicopter Brownout

Previous theses by graduates of the Space Systems curriculum at the Naval Postgraduate School addressed helicopter brownout, each focusing on the prediction, and therefore avoidance of brownout conditions. Similarly, PhLASH and LandSafe are two examples of several research efforts directed towards solving this operational challenge. However, most of these proposed methods are reactive in nature; that is to say, they are

searching for solutions only after the helicopter is about to enter or is already engulfed in the dust cloud. This thesis attempts to provide proactive guidance founded on the principle that the foundation for a successful approach and landing resides in the planning phases.

B. PHYSICAL PROPERTIES OF SOIL

1. General

“Soil conditions can be classified according to their physical, chemical, and biological characteristics, which are developed during soil formation processes” (Makhamreh, 2006, p. 1). Understanding the nature of brownout is therefore predicated by examining these characteristics of the soil present within potential landing zones. “Soil is a mixture of inorganic mineral particles and organic matter of varying size and composition. The particles make up about 50 percent of the soil’s volume. Pores containing air and/or water occupy the remaining volume” (Jensen, 2000, p. 472). The following sections summarize the various and complex characteristics a soil exhibits. The purpose of this thesis is to determine what soil characteristics contribute to helicopter brownout, and if any of these characteristics are remotely distinguishable. To that end, this thesis explores the physical aspects of soil, specifically the soil texture, surface roughness and the soil water content.

2. Soil Texture and Particle Size Distribution

Texture describes a soil’s physical properties, referring to the fineness or coarseness of the individual grains of a soil, and is determined by the relative proportion and size of the grains therein contained. “There are three universally recognized soil grain size classes: sand, silt, and clay” (Jensen, 2000, p. 473). The soil size is further broken down into a particle size distribution; these subcategories are called separates. The size separates used by the Soil Survey Manual (2008, Ch. 3, p. 61) are as follows:

Very coarse sand:	2.0-1.0 mm
Coarse sand:	1.0-0.5 mm
Medium sand:	0.5-0.25 mm
Fine sand:	0.25-0.10 mm
Very fine sand:	0.10-0.05 mm
Silt:	0.05-0.002 mm
Clay:	< 0.002 mm

Figure 2. Size Separates for <2 mm Mineral Material
(From Soil Survey Manual, 2008)

“Soil texture refers to the weight proportion of the separates for particles less than 2 mm as determined from a laboratory particle-size distribution” (Soil Survey Manual, 2008). Sand is the largest particle, and does not form clumps due to its size, among other factors. Silt is similar to flour in texture and its size varies between 0.05-0.002 millimeters in diameter. As the smallest sized particle, clay typically measures less than 0.002 millimeters in diameter, and generally has the greatest capacity to retain water. Although not to scale but rather shown for its comparative relationships, the illustration below also provides a depiction of the sizes of these soil particles, as shown in Figure 3 (Ch. 3, p. 63).

The size separates evaluate only particle size without regard to chemical composition or structural framework. In the Soil Survey Manual (2008), field estimates can evaluate texture through a tactile evaluation (p. 62). “Sand particles feel gritty and can be seen individually with the naked eye. Silt particles cannot be seen individually without magnification; they have a smooth feel to the fingers when dry or wet” (Soil Survey Manual, 2008). According to Brady and Weil (2004), because sand particles are relatively large, so too are the voids between them; this promotes the free drainage of water and entry of air into the soil, which means sand particles can hold little water (p. 97). “The pores between silt particles are much smaller than sand, so silt retains

more water and lets less drain through” (Brady and Weil, 2004, p. 97). Lastly, clay has a large capacity to absorb and hold water, due to their small pore size (Brady and Weil, 2004, p. 98).

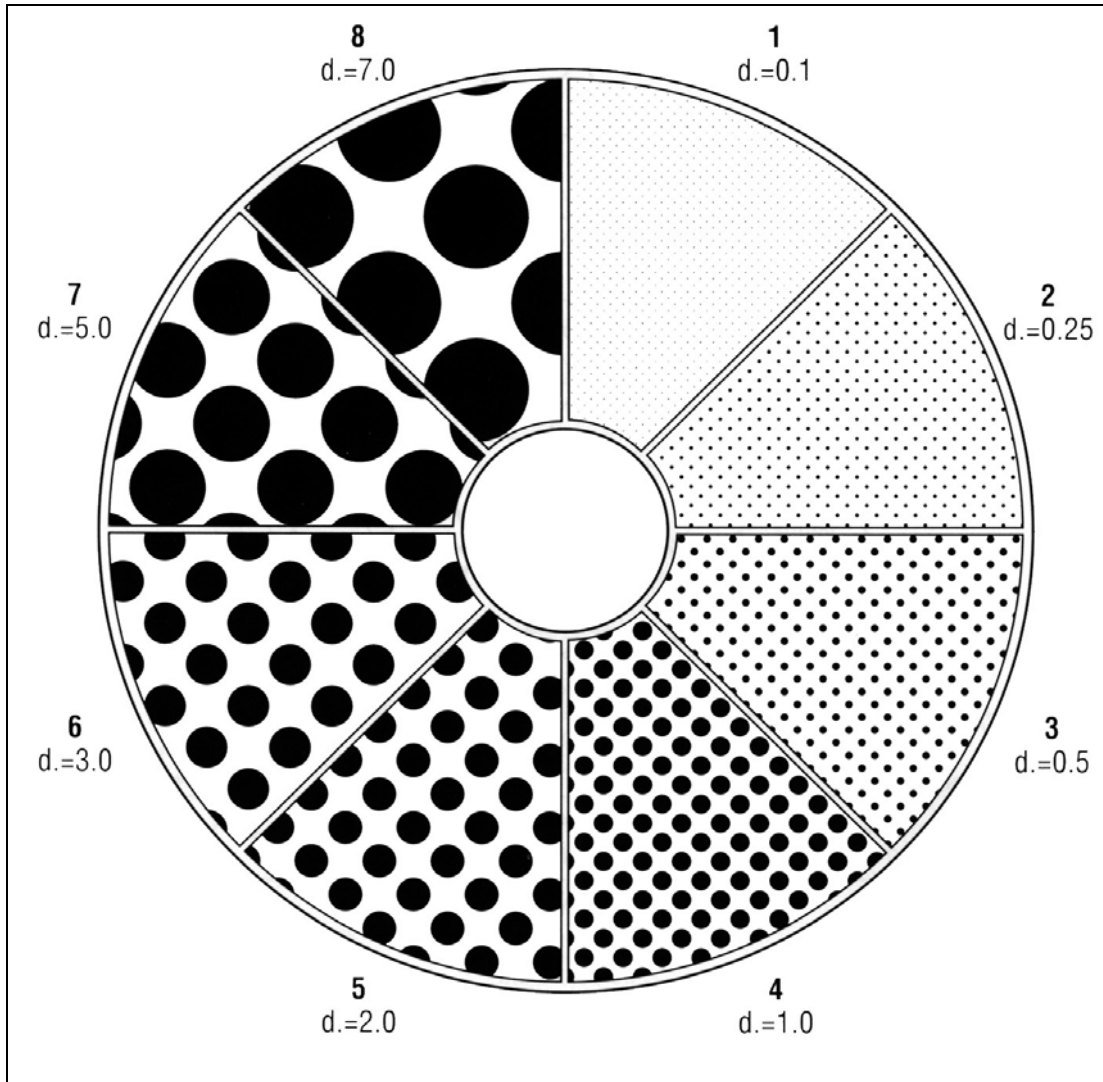


Figure 3. Sizes of particles of indicated diameters (d) in millimeters
(From Soil Survey Manual, 2008)

There is an important distinction between the description of dust particles and the Soil Survey Manual (2008) recognized soil sizes. The Soil Survey Manual states that dust particles are mostly clay and very fine silt (Ch. 3, p. 14). Compare this to sand dunes, which are typically fine or medium sand particles with low amounts of clay. While both can be moved and deposited by the wind, only dust is attributed to being

distributed in large amounts worldwide, because dust can be carried for long distances whereas sand cannot. While sand dunes can be associated with brownout, it is dust with its smaller particulate size that is associated more commonly with helicopter brownout.

These soil textures are combined into texture classes by the Soil Survey Manual (2008): “sand, loamy sands, sandy loams, loam, silt loam, silt, sandy clay loam, clay loam, silty clay loam, sandy clay, silty clay, and clay” (Ch. 3, p. 63). See Figure 4.

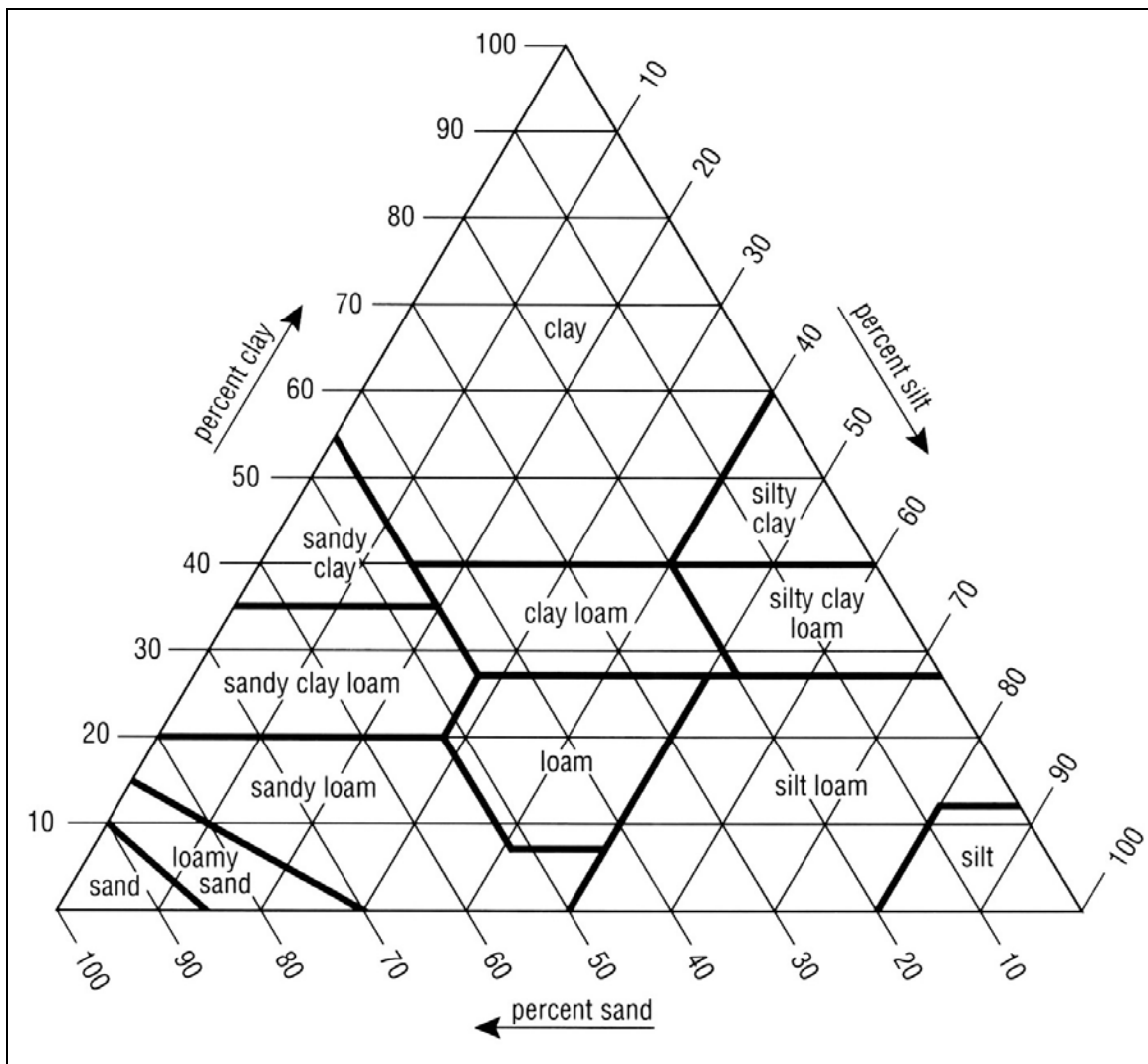


Figure 4. Percentages of clay, silt, and sand in the basic textural classes (From Soil Survey Manual, 2008)

For the purpose of this thesis, the focus will be on loamy sand and sandy loam (located in the lower left corner of the triangle), as they are soil textural classes that exist within the research region of the Yuma Proving Grounds (Miller, Borchers, Hendricksx, Hong, Lensen, Schwering, and Rhebergen, 2002, p. 282). A loam is defined as an ideal mixture of sand, silt and clay particles. Thus while most soils are some type of loam, a loam in which sand is dominant is described as a sandy loam (Brady and Weil, 2004, p. 99). The Soil Survey Manual (2008) describes loamy sand as having “a total of 25 percent or more very coarse, coarse, and medium sand and a total of less than 25 percent very coarse and coarse sand, and less than 50 percent fine sand and less than 50 percent very fine sand” (Ch. 3, p. 64). Similarly, sandy loam is defined as having “a total of 30 percent or more very coarse, coarse, and medium sand, but a total of less than 25 percent very coarse and coarse sand and less than 30 percent fine sand and less than 30 percent very fine sand; or a total of 15 percent or less very coarse, coarse, and medium sand, less than 30 percent fine sand and less than 30 percent very fine sand with a total of 40 percent or less fine and very fine sand” (Soil Survey Manual, 2008, Ch. 3, p. 64).

The question then becomes which of these soil grain sizes are susceptible to becoming airborne by winds due to downwash. Generally, the cascading due to wind goes as follows: the coarse sands and very coarse sands (>0.5 mm) usually only enter the wind stream briefly until they are pulled back down to the ground by gravity. This causes them to impact other soil particles, energizing the finer sands (0.07 mm-0.5 mm) to rise above the surface of the ground higher and stay in suspension longer. Also energized are the silts (0.02 mm-0.07 mm), which remain suspended for long periods of time and can be carried great distances by the wind (Saxton, Chandler, and Schillinger, 1999). This is illustrated below in Figure 5.

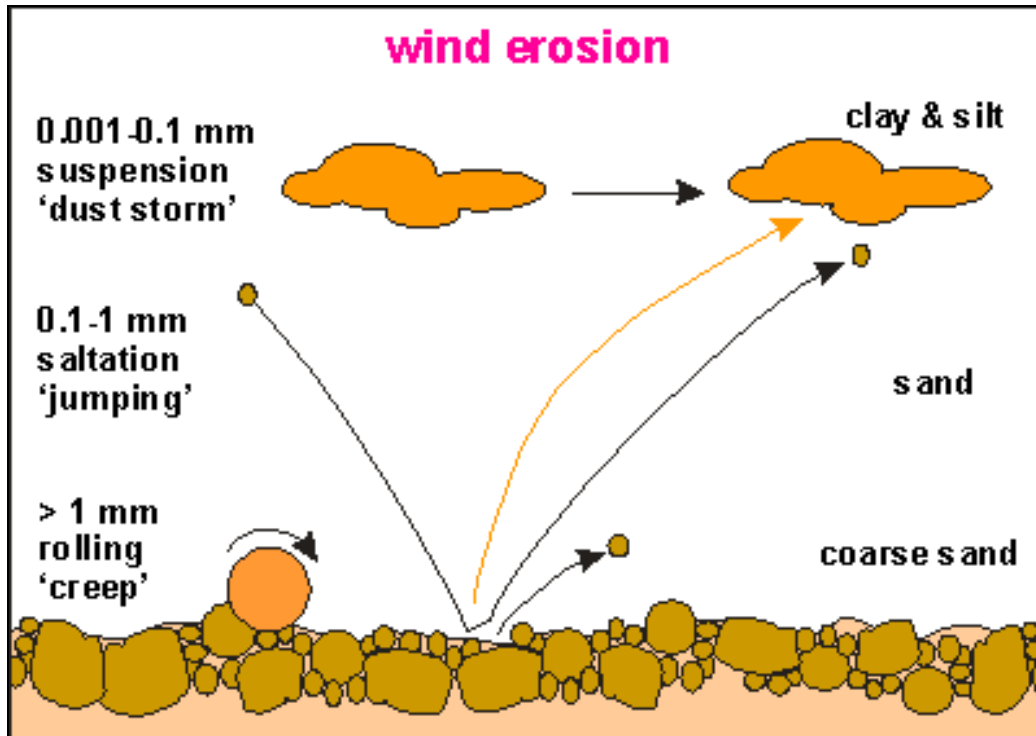


Figure 5. Effects of Wind Erosion
(From Anthoni, 2000)

Even without studying soil science, the average person can presume that helicopter brownout occurs within an arid climate that is devoid of vegetation and characterized by sandy particles. The Blackhawk incident detailed in the first section illustrates that scenario. Such climatic conditions also describe most of the current areas of responsibility for military operations. It would follow, then, that texture and particle size distribution are certainly indicators of helicopter brownout.

3. Surface Roughness

“Several different criteria exist to decide if a surface is ‘smooth’ or ‘rough’” (Elachi and van Zyl, 2006, p. 204). “Surface roughness is the terrain property that strongly influences the strength of the radar backscatter” (Jensen, 2000, p. 308). The Soil Survey Manual (2008) states that roughness pertains to the ground surface without including vegetation (Ch. 3, p. 9). It also states that the roughness of the reflecting surface affects the amount of reflected light, particularly if the incidental light is nearly at a right angle (Ch. 3, p. 9). According to Henderson and Lewis (1998), there are three

general approximations employed to categorize a surface as rough or smooth. The first “rule of thumb” is a rough estimate which uses $\lambda/10$, where λ is the wavelength of the system. A more accurate approximation of surface roughness is defined by the Rayleigh Criterion, where the surface irregularities are expressed as average height variations (h_{rms}) and categorization is dependent on wavelength (λ) or look angle (ϕ)” (p. 158). “According to the Raleigh Criterion, a surface is rough if

$$h_{\text{rms}} > \lambda / 8 \cos \phi$$

For example, for a surface to appear rough on a radar imagery with the following parameters: $\lambda = 23.5$ cm and $\phi = 21$, it must exhibit an average surface roughness greater than 3.2 cm” (Henderson and Lewis, 1998, p. 158). The third and most accurate approximation uses the following two equations to define the boundary between smooth, intermediate, and rough:

$$h_{\text{rms}} > \lambda / 25 \cos \phi \text{ for when a surface is considered smooth}$$

$$h_{\text{rms}} < \lambda / 25 \cos \phi \text{ for when a surface is considered rough}$$

Any height variation that lies between these values is considered to be of intermediate roughness (Henderson and Lewis, 1998, p. 159). Essentially, it is the geometry of the air-soil boundary and can vary dramatically. The wavelength and look angle will be defined in Chapter II, Section D Polarimetric Radar.

“In general, radar backscatter increases with increasing surface roughness” (Henderson and Lewis, 1998, p. 34). The hypothesis is that the lack of return (i.e., darker) indicates the soil size is finer and therefore more likely to cause helicopter brownout. This author will use polarimetric radar to explore if the finer particles will result in less energy returned to the sensor for a corresponding lower digital number (DN) (e.g., appear darker) than would be apparent with a rougher soil that would exhibit more backscatter.

4. Soil Water Content and the Correlation with Dielectric Constant

The ratio of the mass of water to the mass of dry matter in a given soil sample is known as soil moisture content, or soil water content, indicating the ability of the soil to hold or transmit water. Soil water content is another key parameter when remotely analyzing a soil and is chiefly determined from the particle size distribution. Soil particle size affects soil water content because particle size determines how much space is present between soil particles. This void, called soil pore space, allows water and air to penetrate the soil (Soil Survey Manual, 2008, Ch. 3, p. 104). “There is a relationship between the size of the soil particles found in a mass of soil (e.g., 1 m³) and the amount of moisture that the soil can store” (Jensen, 2000, p. 476). Fundamentally, the amount of water maintained depends on the size and arrangement of the soil pores. For coarse and loose soils, water is able to move freely through the soil due to gravitation forces and drains away leaving only a small trace. On the other hand, fine-textured soils like clay have a larger concentration of smaller pores resulting in more pore space and, therefore, retain larger amounts of water (Gupta and Jangid, 2008, p. 885). It is natural to assume that the drier the soil, the more susceptible it is to brownout. Conversely, higher moisture content within a soil effectively reduces the amount of dust particulates that may be swept into the air, and thus minimizes the likelihood of brownout.

The moisture content of the soil is the most significant factor that determines the dielectric constant, which is defined as a measure of soil’s ability to conduct electrical energy (Jensen, 2000, p. 311). Key to this research is the fact that water has a high microwave dielectric constant; dry soils have a low dielectric constant (Elachi and van Zyl, 2006, p. 174).

Different soil types vary in dielectric constant values as a function of soil moisture; therefore, soil reflectivity is linked to the soil moisture content by the dielectric constant (Elachi and van Zyl, 2006, p. 174). “Dry soil surfaces have dielectric constants on the order of 2 to 3, whereas water has a dielectric constant of approximately 80 at microwave frequencies. Therefore, adding a relatively small amount of water to the soil drastically changes the value of the dielectric constant” (Elachi and van Zyl, 2006, p. 207). The dielectric constant affects the amplitude of the radar return, the backscatter in

particular, causing wet objects to appear bright and dry objects to appear dark. As the following illustration shows, absorption increases with moisture content, while reflection (backscatter) will increase as dielectric constant increases.

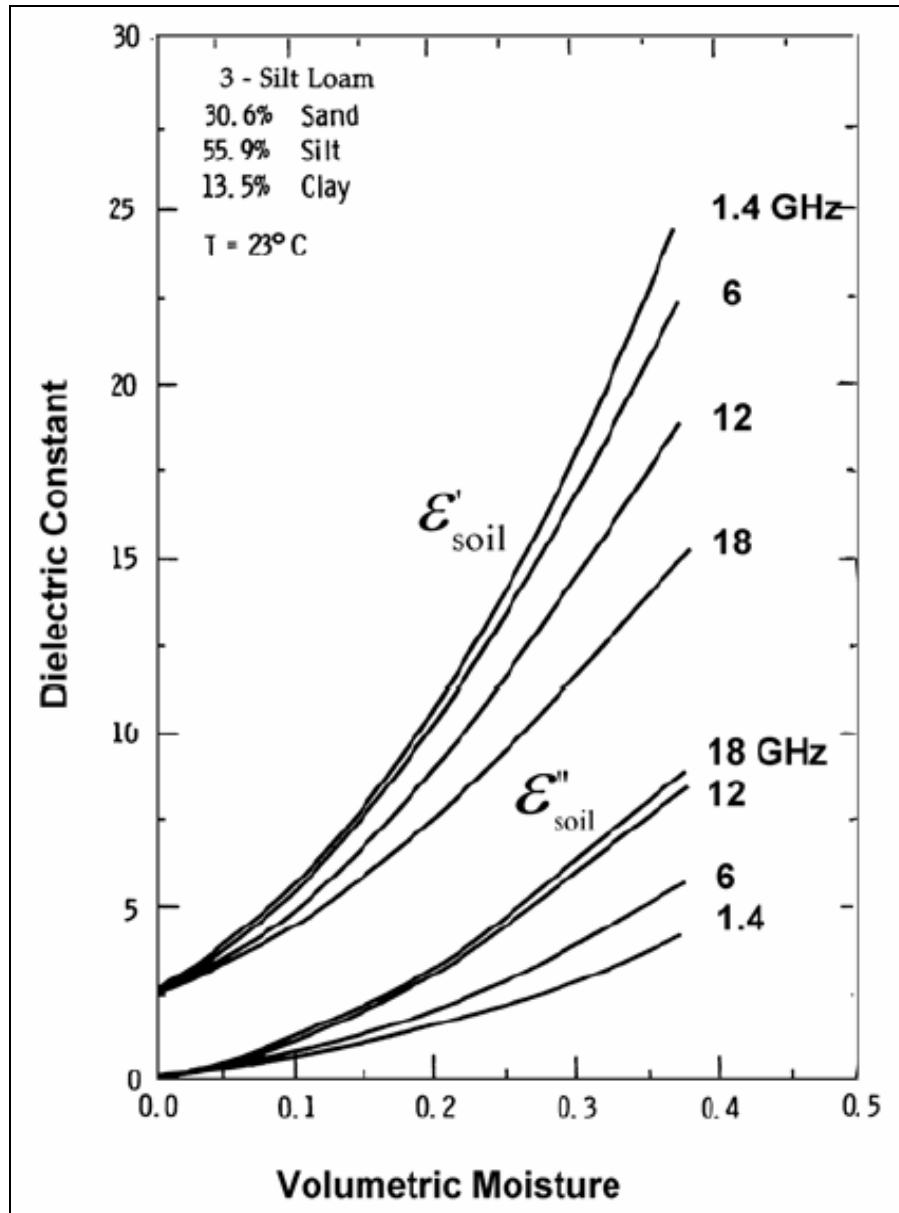


Figure 6. The dielectric constant as a function of water content
(From Olsen, 2007, p. 192)

Note that the real component, denoted by ϵ' , applies to reflectance while the imaginary component (ϵ'') applies to the penetration. As the soil moisture increases, so does the imaginary component of the dielectric constant, which translates to an increased absorption of the radar energy (Olsen, 2007, p. 192). Therefore, it is anticipated for dry soil to appear dark in a radar return due to the absorption of the radar energy.

5. Soils, Thesis Specific

While there are several classes that define soil water content (dry, moist, wet), it is beyond the scope of this thesis to define them; rather, it is more important to know that moisture affects the spectral reflectance of the soil and therein lies the emphasis. The same holds true for surface roughness as well as for the dielectric constant. While each of these affects the soil's reflectance by the radar system, to define them further detracts from the objective of the thesis. The key finding is that the spectral reflectance of soils is a function of several important characteristics, and the key characteristics with respect to polarimetric radar in this thesis addressed herein are the particle size distribution, surface roughness and soil moisture content.

C. REMOTE SENSING VIA THE ELECTROMAGNETIC SPECTRUM

1. Electromagnetic Spectrum

“The chief thing to understand is the electromagnetic (EM) spectrum and EM radiation, of which light, radar, and radio waves are examples” (Olsen, 2007). If electromagnetic radiation is defined as the energy that propagates through space (or material media) in the form of an advancing interaction between the electric and magnetic fields, then the electromagnetic spectrum describes the wavelengths and frequencies of the different types of energies (“Radar and Stereoscopy,” 2007). Below is an illustration of an electromagnetic wave (Figure 7).

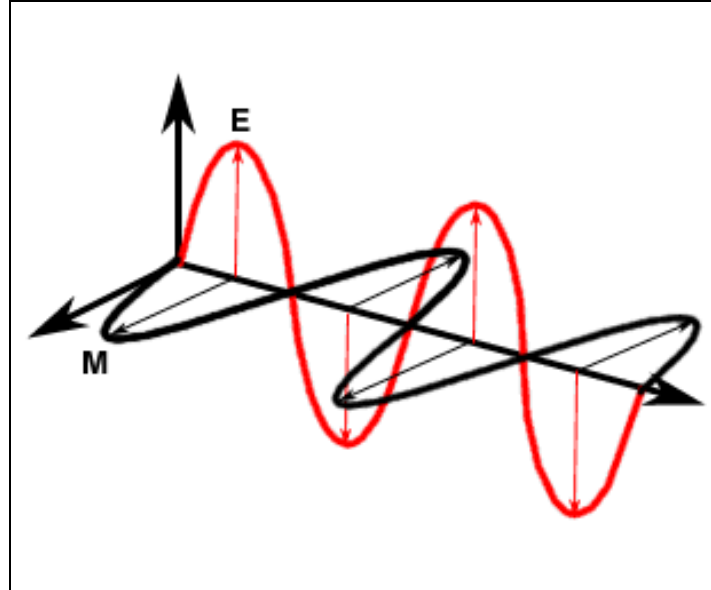


Figure 7. Illustration of an electromagnetic wave, where M is the magnetic field and E is the electric field
(From “Glossary of Remote Sensing Terms,” 2005)

When EM radiation strikes matter, it is called incident radiation. This incident radiation can be transmitted (also referred to as refracted), reflected, absorbed, or scattered (Figure 8). Transmission through material media of different densities causes the incident radiation to be refracted. Reflection occurs when incident radiation is bent from the smooth, mirror-like surface in a single predictable direction, such as a body of water. Incident radiation is taken in by an opaque material and is called absorption. Lastly, scattering occurs when the incident radiation is spread out in many unpredictable directions, including the direction from which it originated. “Scattering occurs with surfaces that are rough relative to the wavelengths of incident radiation” (Olsen, 2007, p. 49–52).

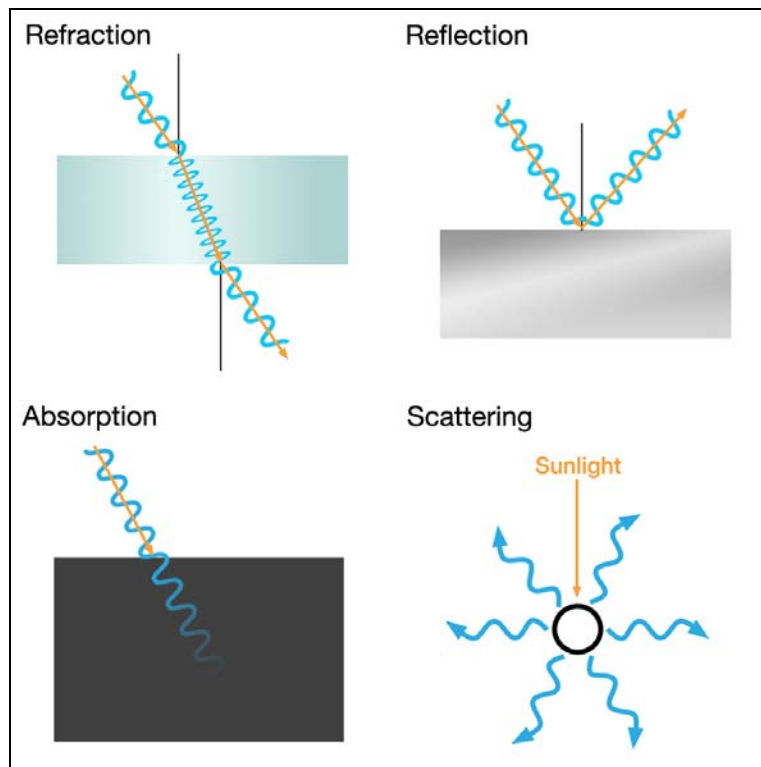
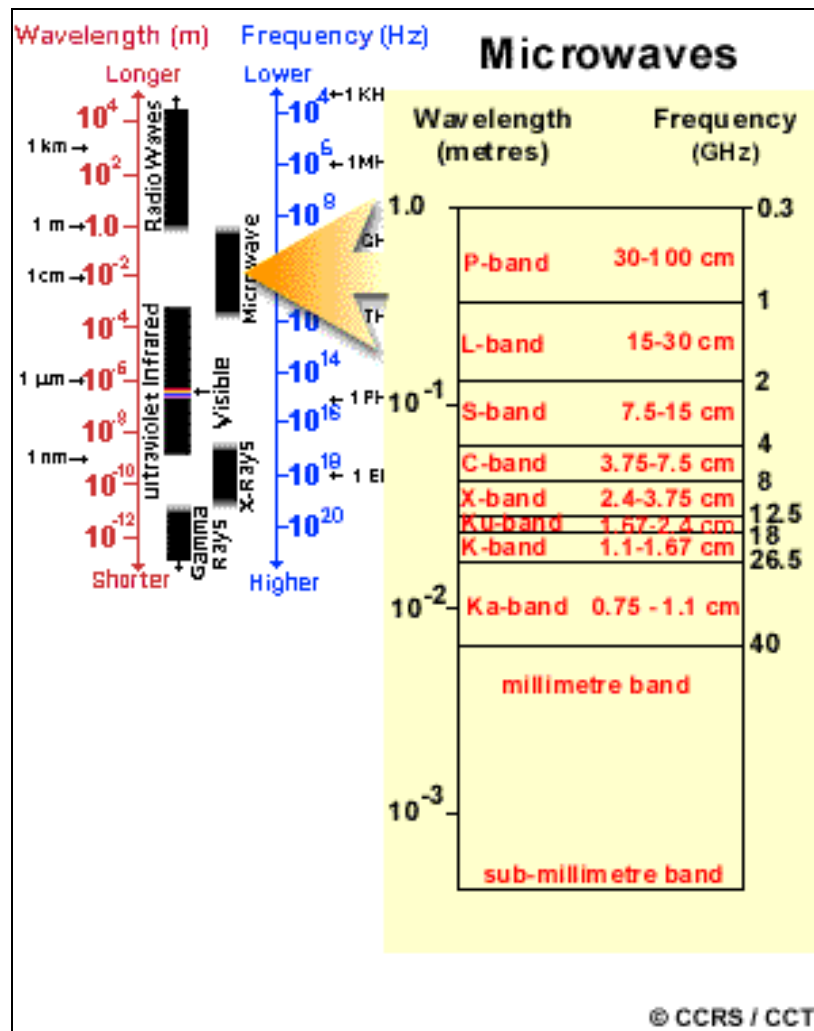


Figure 8. Four interactions of electromagnetic radiation
(From “Photodermatology/Photobiology,” 2008)

2. Imaging Radar

Radar was chosen as the primary sensor due to distinct advantages of its electromagnetic properties. An active imaging radar system transmits short pulses of EM energy, and records the backscattered energy received by the system. Because the radar system creates its own energy, it does not need sunlight for illumination, nor is radar inhibited by atmospheric conditions, unlike visible and infrared imagery systems.

Radar works in the microwave portion of the EM spectrum (Figure 9). “The longest microwave is approximately 2,500,000 times as large as the smallest visible light wave. Radar band designations range from the Ka band occurring between 7.5 and 11.0 mm to the P band range between 30 and 100 cm” (“Radar and Stereoscopy,” 2007).



radar antenna” (“Glossary of Remote Sensing Terms,” 2005). While portions of the incident radar energy may be reflected or absorbed, it is the backscatter that is measured and recorded for purposes of producing imagery. “It is the effects of terrain on the radar signal that we are most interested in, i.e., the amount of radar cross-section, σ (sigma), reflected back to the receiver, per unit area (A) on the ground. This is called the *radar backscatter coefficient* σ° (sigma naught) and is computed as:

$$\sigma^\circ = [\sigma / A]$$

The radar backscatter coefficient determines the percentage of electromagnetic energy reflected back to the radar from within a resolution cell, e.g., 10 x 10 m. The actual σ° for a surface depends on a number of terrain parameters, like geometry, surface roughness, moisture content, and the radar system parameters (wavelength, depression angle, polarization)” (Jensen, 2000, p. 308).

Therefore, a digital radar image is the two-dimensional representation of pixels such that the intensity (or brightness) of each pixel is proportional to amount of backscatter (Jansen, 2000, p. 308). For a typical image processing system with eight bits of dynamic range, each pixel is represented by a value based upon a radiometric scale of 256 values, also known as the digital number (DN) (Olsen, 2007, p. 142).

D. POLARIMETRIC RADAR

While it is beyond the scope of this thesis to provide specific details of the science behind radar polarimetry, it is necessary to introduce general concepts of radar polarimetry to understand the analysis of the resulting images. This author will be focusing on those aspects that were central to helicopter brownout research, specifically soil texture, surface roughness, and dielectric constant.

The remainder of this section is from the Canada Centre for Remote Sensing (CCRS) Web site, specifically from the Glossary of Remote Sensing Terms defining Radar Polarization.

Polarization refers to the geometry of the tip of the electric vector (E) as it evolves with time (as opposed to the magnetic field vector (M)). Remote sensing radars are

usually designed to transmit either vertically polarized or horizontally polarized radiation. This means that the electric field component of the wave lies in a vertical plane or a horizontal plane, where “vertical” and “horizontal” is defined relative to a reference such as the plane tangent to the Earth’s surface. Likewise, the radar can receive either vertically or horizontally polarized radiation, and sometimes both. The planes of transmitted and received polarization are designated by the letters H and V for Horizontal and Vertical. Thus the polarization of a radar image can be HH, for horizontal transmit, horizontal receive, VV for vertical transmit, vertical receive, HV for horizontal transmit vertical receive, and vice versa. See Figure 10.

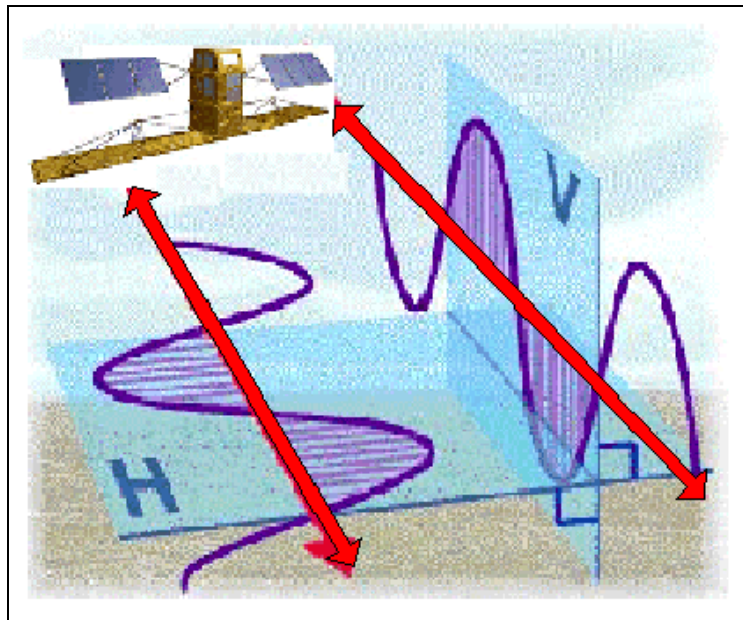


Figure 10. Radar systems create polarized EM waves
(After “Glossary of Remote Sensing Terms,” 2005)

When the polarization of the received radiation is the same as the transmitted radiation, the resulting image is said to be like-polarized or co-polarized. When the polarization of the received radiation is orthogonal to the transmitted radiation, the image is said to be cross-polarized. Cross-polarized signals are usually a result of multiple scattering by the target or terrain, and tend to result in weaker backscatter than like-polarized signals.

The polarization is established by the radar antenna, which is configured to have different signal paths on transmit and on receive. The backscatter of microwaves from an object depends on the relationship between the polarization of the incident wave and the geometric structure of the object. When polarimetric data is collected from the object, much more information is obtained than with a single-channel radar.

To illustrate the effect of polarization, consider the very simple model of a vegetation canopy consisting of short vertically linear scatterers over a rough surface, as shown in Figure 11. Assuming that the linear scatterers will act as short vertical dipoles, then incident vertical electromagnetic (EM) waves will backscatter from the vegetation and little energy will reach the ground. Conversely, the horizontally polarized incident wave will mainly pass through the vegetation and scatter from the ground. Therefore, the received vertical signal will depend more on the scattering behavior of the vegetation while the received horizontal signal will depend more on the scattering behavior of the ground.

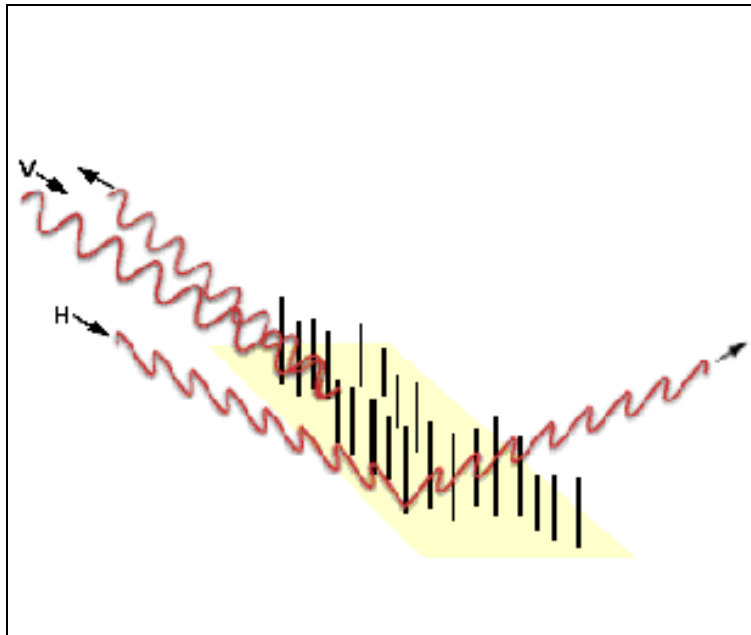


Figure 11. Illustration of how vertically polarized waves are backscattered by vertical dipoles, while horizontally polarized waves pass through the dipoles and are scattered by the ground underneath
(From “Glossary of Remote Sensing Terms,” 2005)

Quadrature Polarization Radar is a radar system designed to collect image data of a scene using two orthogonal transmit polarizations and the same two polarizations on receive. Polarimetric radar is a synonym. The term is sometimes shortened to “Quad Pol Radar,” where the term “quad” refers to the fact that the transmit and receive channels are in quadrature (i.e., orthogonal), and there are four channels required to make the measurements (typically HH, HV, VV & VH). The four channels must be received closely enough in space and time so that the channels are mutually phase coherent. When these four channels are measured, the scattering matrix of the reflectivity of each pixel is obtained, and other polarimetric descriptors such as the polarization signature can be computed.

There may be confusion with the term “quad pol radar.” The latter term refers to a radar system in which **four** polarizations are received in orthogonal or **quadrature** pairs, in near-simultaneous operation, and the channels are mutually phase coherent. In contrast, a multi-polarization radar system can have two to four possible polarizations, which are not necessarily phase coherent or simultaneous. A multi-polarization radar may have only one channel, which is switchable between different polarizations. In general, a multi-polarization radar is a cheaper alternative to a quadrature polarization radar, while possessing some of the advantages of the latter.

E. BASICS OF RADAR IMAGE INTERPRETATION AND ANALYSIS

This section is adapted from the Canada Centre for Remote Sensing (CCRS) Web site, specifically from the tutorial titled “Fundamentals of Radar Remote Sensing.”

Most remote sensing data is recorded in digital format, necessitating that the image interpretation and analysis incorporates digital image processing. Obviously, in order to do digital processing, there needs to be an image analysis system, with the appropriate hardware and software to process the data. A commonly used, commercially available digital processing system is Environment for Visualizing Images (ENVI) software, developed specifically for remote sensing image processing and analysis.

While there are several image processing functions available within this image analysis system, this research focused on the following three functions: Preprocessing, Image Transformation, and Image Classification/Analysis.

1. Research Image Analysis System

The computational tool used in the development of this research was the Environment for Visualizing Images (ENVI) software. It was created by Research Systems Incorporated (RSI), and is currently owned by ITT Visual Information Solutions (ITT VIS). ENVI is an image processing system, commonly utilized by those who work with satellite remote sensing data (Research Systems, Inc., 2005, p. 2). ENVI is written in Interactive Data Language or IDL, which allows for flexibility in programming for integrated image processing (Research Systems, Inc., 2005, p. 3). The ENVI module titled SARscape is an add-on feature that allows an analyst the ability to read, process, analyze and output radar data, as well as integrate the information with other geospatial data and tools.

2. Preprocessing Function

Preprocessing functions involve those operations that are normally required prior to the main data analysis and extraction of information, and this research focused mainly on geometric corrections. Geometric corrections include correcting for geometric distortions due to sensor-Earth geometry variations, and conversion of the data to real world coordinates (e.g., latitude and longitude) on the Earth's surface. This research georeferenced the radar image using ENVI SARscape.

3. Image Transformation

Image transformations involve combined processing of data from multiple spectral bands. Operations are performed to combine and transform the original bands into new images, which better display or highlight certain features in the scene. This research utilized a procedure called Principal Components Analysis, which is used to more efficiently represent the information in multichannel imagery.

Principal Component Transform, also known as Principal Component Analysis (PCA), is defined by the Canada Centre for Remote Sensing (“Glossary of Remote Sensing Terms,” 2005) as “a digital image enhancement technique that transforms spectral radiance values of the original, correlated image data sets into new, uncorrelated data sets.” In other words, PCA concentrates the information common to correlated data sets. The objective of this transformation is to reduce the dimensionality (i.e., the number of bands) in the data, and compress as much of the information in the original bands into fewer bands. The ‘new’ bands that result from this statistical procedure are called components (“Fundamentals of Remote Sensing,” 2007). Rotating the data space into a coordinate system in which the different bands are uncorrelated can lead to a useful transformation for the detection of targets or other tasks such as classification (Olsen, 2007, p. 151). The CCRS “Glossary of Remote Sensing Terms” also states that performing a PCA before classifying the image data can expedite the process as well as increase the accuracy of the classification (2005).

The procedure used in the IDL code written by Dr. R. C. Olsen to use the Principal Component Transform was first described by J. S. Tyo, E. N. Pugh, Jr., and N. Engheta. In their article, they describe the strategy for representing polarization information for mapping into pseudo-color images. “The new mappings are demonstrated to be more robust for presenting reliable information to human observers...” (Tyo, Pugh Jr., & Engheta, 1998, p. 367).

After applying the Principal Component Transform, a color image can be produced by assigning each of the principal components to a color band. A commonly used color space is the Red-Green-Blue (RGB) color space, which is optimized for computer screens (“Glossary of Remote Sensing Terms,” 2005). Likewise, the IHS or the Intensity-Hue-Saturation color scheme is a system that produces color imagery that is adapted to human vision. In an IHS color space, the first component is intensity or color brightness, the second component is hue or the actual color, and the third component is saturation or the purity of the color (Olsen, 2007, p. 152).

4. Image Classification and Analysis

Image classification and analysis operations are used to digitally identify and classify pixels in the data. For illustration, Figure 12 shows classification performed on multi-channel data sets (A), and this process assigns each pixel in an image to a particular class (B) based on statistical characteristics of the pixel brightness values (Figure 12).

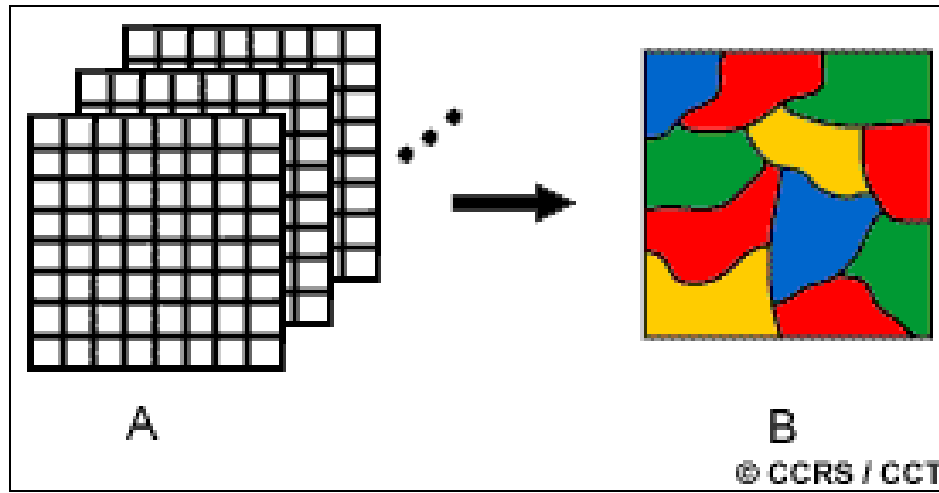


Figure 12. Basic illustration of classification of multi-channel data sets (A) by pixel into classes within an image (B)
(From “Fundamentals of Remote Sensing,” 2007)

While there are a variety of approaches taken to perform digital classification, two generic approaches which are used most often are supervised and unsupervised classification. This research used unsupervised classification, described below.

First, it is necessary to define and distinguish information classes from spectral classes. Information classes are those categories of interest that the analyst is actually trying to identify in the imagery, such as different kinds of crops, different forest types or tree species, different geologic units or rock types, etc. Spectral classes are groups of pixels that are uniform (or near-similar) with respect to their brightness values in the different spectral channels of the data. The objective is to match the spectral classes in the data to the information classes of interest. Rarely is there a simple one-to-one match between these two types of classes. Rather, unique spectral classes may appear which do

not necessarily correspond to any information class of particular use or interest to the analyst. Alternatively, a broad information class (e.g., forest) may contain a number of spectral sub-classes with unique spectral variations. Using the forest example, spectral sub-classes may be due to variations in age, species, and density, or perhaps as a result of shadowing or variations in scene illumination. It is the analyst's job to decide on the utility of the different spectral classes and their correspondence to useful information classes.

Common classification procedures can be broken down into two broad subdivisions based on the method used: supervised classification and unsupervised classification. In a supervised classification, the information classes are identified first and then used to determine the spectral classes which represent them. This assumes the analyst knows a priori the soils characteristics of the radar image; however, this research did not previously know which soil characteristics that were conducive to helicopter brownout, so the procedure employed was the unsupervised classification.

The unsupervised classification process first groups the spectral classes, based on the statistical information in the data. These are then matched by the analyst to information classes (if possible). Algorithms are used to determine the reasonable groupings in the data. Typically, the analyst specifies how many groups are to be looked for in the data; this technique was applied in this research. The final outcome of this iterative grouping process may result in some groups that the analyst will want to subsequently combine, or groups that should be broken down further. Each of these will likely require an adjustment to and reapplication of the algorithm. Therefore, unsupervised classification is not completely without human intervention.

In the following illustration of unsupervised classification in Figure 13, the analyst first groups the data by digital number (DN), and then applies the algorithm. With the spectral classes grouped, the analyst can then assign the classes that best identify the data, meaningful ground categories. Its value is largely as a guide to the spectral content of a scene to aid in making a preliminary interpretation as the precursor to conducting more meaningful supervised classification procedures. This research serves as that preliminary interpretation.

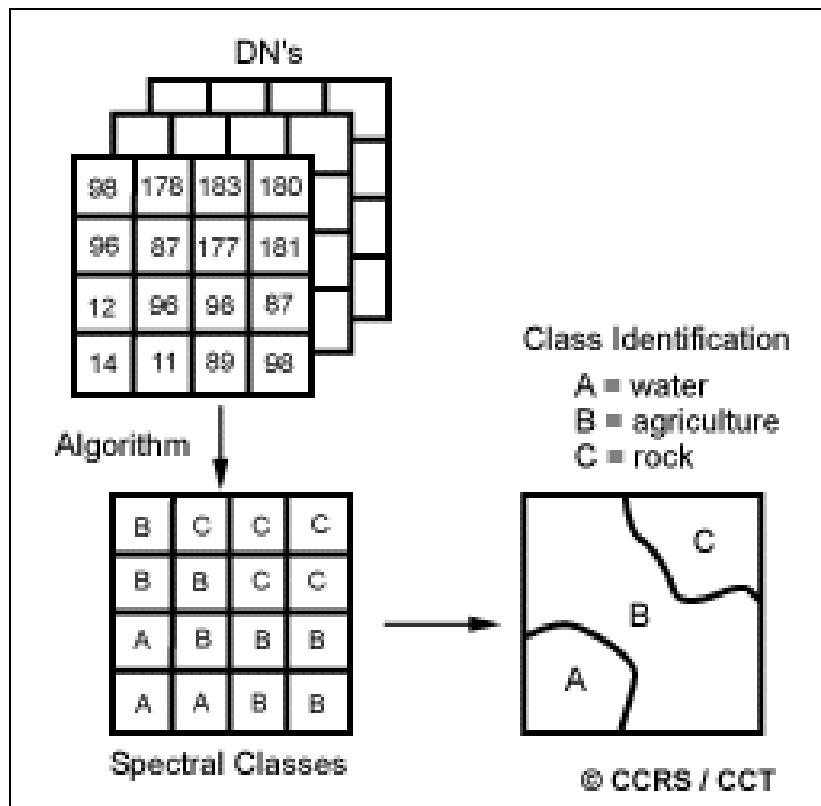


Figure 13. Illustration of Unsupervised Classification
(From “Fundamentals of Remote Sensing,” 2007)

F. REMOTE SENSING TECHNOLOGY

1. RADARSAT-2

While the mechanics of the radar system on RADARSAT-2 are important, they were not the focus of this research. Therefore, only the basic characteristics of the satellite and a generic description of its polarimetric radar are discussed. The information about RADARSAT-2 detailed below was found on MacDonald, Dettwiler, and Associates, Limited (MDA) Web site (2008).

RADARSAT-2, launched on 14 December 2007, is Canada’s second polarimetric radar satellite. While it was a collaboration between the Canadian government and the Canadian satellite industry, the agency responsible for the operations of the satellite is

MDA. The Synthetic Aperture Radar (SAR) payload onboard is capable of providing three-meter high resolution, as well as 100-meter low-resolution images. This sensor operates on a single microwave frequency of 5.405 gigahertz (C-band) and has an imaging capacity of 28 minutes per orbit. This near-polar, sun synchronous satellite is travelling at an altitude of 798 kilometers above the Earth's surface, crossing the equator at dawn and again at dusk. An artist depiction of RADARSAT-2 is shown in Figure 14.

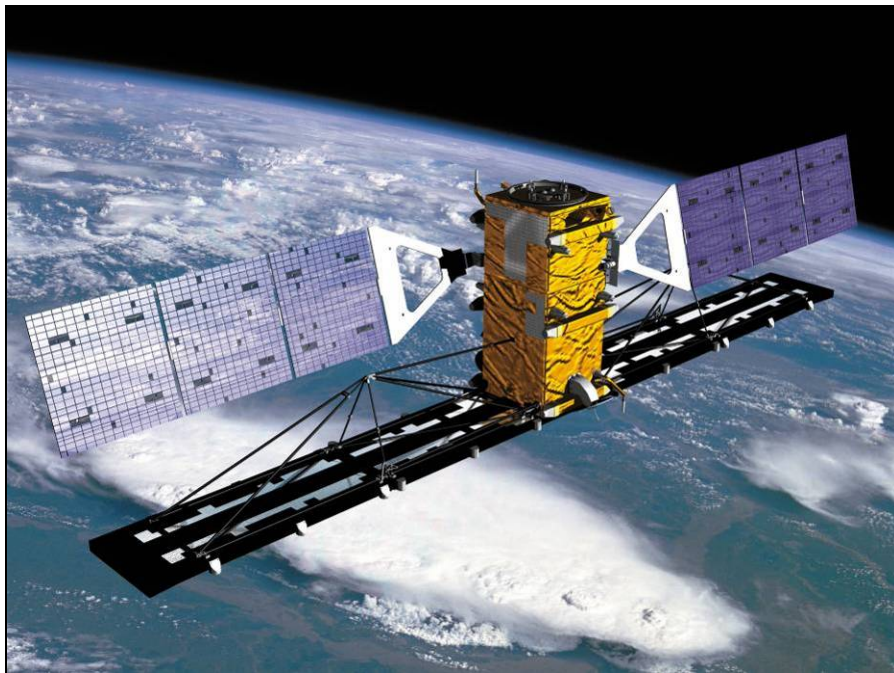


Figure 14. Artist Depiction of RADARSAT-2
Artwork © MacDonald, Dettwiler and Associates, Ltd. 2009
All Rights Reserved

2. RADARSAT-2 Product Types

There were many product types that RADARSAT-2 is capable of producing; addressed herein is Single Look Complex (SLC). Specifically, SLC is data that retains the phase and amplitude information of the original SAR data. SLC product data is stored in slant range, and is corrected for satellite reception errors, includes latitude/longitude positional information. In addition, SLC data retains the optimum resolution available for each beam mode. The beam mode for this research was Fine

Quadrature Polarization, which has a nominal swath width of 25 kilometers, with an approximate resolution of 8 meters. The imagery available from satellites like RADARSAT-2 provides a tremendous opportunity to show the impact of polarimetric radar imagery data for better discrimination of various surface types.

RADARSAT-2 provides an opportunity to accomplish terrain classification for military applications. In the current military operations, often the landing zones are in denied areas and remote sensing provides an efficient and reliable means of gathering the necessary information.

3. Science and Operational Applications Research

SOAR, or Science and Operational Applications Research for RADARSAT-2, is a joint partnership program between MDA and the Canadian government through the Canadian Space Agency (CSA) and the Canada Centre for Remote Sensing (CCRS). The SOAR program, through a loan of limited amounts of RADARSAT-2 data to research projects, provides an opportunity to explore the capabilities of the satellite and its sensors. The main objective is to explore operationally and commercially viable solutions to current problems and issues (“Science and Operational Applications Research for RADARSAT-2,” 2009). This research obtained data from this program.

III. DESCRIPTION OF DATA COLLECTION

A. RESEARCH AREA OF INTEREST

1. Location

Yuma Proving Grounds (YPG) in Yuma, Arizona was chosen as the research area of interest. It was chosen because of its similarity to current military areas of operation, such as Iraq and Afghanistan. However, it will likely have utility to prevent accidents due to brownout in other areas of operations including arid environments as well as non-arid regions. The research area of interest was roughly defined initially as:

LATITUDE (NORTH)	LONGITUDE (WEST)
33° 18' 53.76"	114° 17' 8.86"
33° 24' 20.45"	114° 15' 55.85"
33° 21' 38.70"	114° 15' 31.01"
33° 21' 40.38"	114° 16' 41.26"

Table 1. The Area of Interest (Latitude/Longitude) of Yuma Proving Ground

2. Area of Interest Specifics

YPG Landing Zone 1 has been identified as a landing zone highly prone to brownout. The center of this thousand meter landing zone is located approximately at Latitude/Longitude of North 33° 23' 45.8"/West 114° 16' 34.5". Figure 15 below is a optical image of YPG, which also shows this landing zone (left of center, dark colored area, denoted by the yellow box). This landing zone area had been deliberately prepared by tilling the area repeatedly as part of the Defense Advanced Research Project Agency's Sandblaster research, which is ongoing and still working to solve the brownout dilemma.



Figure 15. Research area of interest within Yuma Proving Ground, where the yellow box indicates the landing zone which is highly susceptible to brownout
(From Google Earth, 2009)

B. RADARSAT-2 DATA SET

The RADARSAT-2 data set was supplied by MDA as part of the CSA SOAR program. The product identifier was PDS_00188310, which contained Single Look Complex data from the Fine Quadrature Polarization (HH, VV, HV, VH) beam mode. A nominal RADARSAT-2 radar image covers an area of approximately 25 kilometers by 25 kilometers. The raw data start time was 22 August 2008 at 13:39:51.492798 Zulu.

IV. OBSERVATIONS AND ANALYSIS

A. METHOD OVERVIEW

The purpose was to develop a classification algorithm generated by polarimetric radar data to predict brownout-type soil conditions. To this end, the general outline of the investigative methodology employed during this research is detailed below. Each step will be discussed in detail in the following sections, but the methodology incorporated the following steps:

- 1) Obtained RADARSAT-2 data set.
- 2) Radar data was georeferenced the data using ENVI SARscape software.
- 3) Using ENVI, the radar image was transformed by compression that reduced the overall file size of the radar image, and created a more visually accessible image.
- 4) Areas of Interest were located within the compressed radar image by visual analysis. An area likely to cause brownout, and another unlikely to cause brownout were examined. In general, the brownout area tended to appear ‘darker’ than the non-brownout areas.
- 5) Using ENVI, histograms were created to determine the distribution of digital numbers throughout the entire scene for each of the cross- and co-polarization images. It was observed that the histograms of the co-polarized images tended to have a shape indicating two types of materials making up the scene being investigated.
- 6) The two peaks of the histogram of the co-polarized images were used to determine threshold values, and the imagery was partitioned using these thresholds.
- 7) Using the ENVI density slice function, the image was colorized using the defined threshold values. The two peaks of the histogram seem to correlate to brownout and non-brownout areas.

8) These steps were applied to the original, uncompressed radar image, producing results that show brownout and non-brownout areas in the image.

B. PROCURE RADAR DATA SET

RADARSAT-2 data set was supplied from MacDonald, Dettwiler and Associates, Limited (MDA) as part of the CSA SOAR program.

C. GEOREFERENCE THE RADAR DATA

The image was georeferenced using an add-on to the ENVI software called SARscape, specifically designed for analyzing synthetic aperture radar images. Georeferencing (also known as geocoding) is the process of converting each pixel from the slant range geometry of the radar system to a map coordinate system. This process is achieved by utilizing data from a Digital Elevation Model, or DEM, which is used to convert the image. This is an important step prior to any other procedures, as it corrects for any geometric distortions of the image information. A typical DEM is UTM-32 in WGS-84 system. This means that the radar image file received from RADARSAT-2 can be directly associated to precise latitude and longitude coordinates on the ground in Yuma. Below is the georeferenced polarimetric radar image in grayscale of the area of interest within the Yuma Proving Ground (Figure 16).

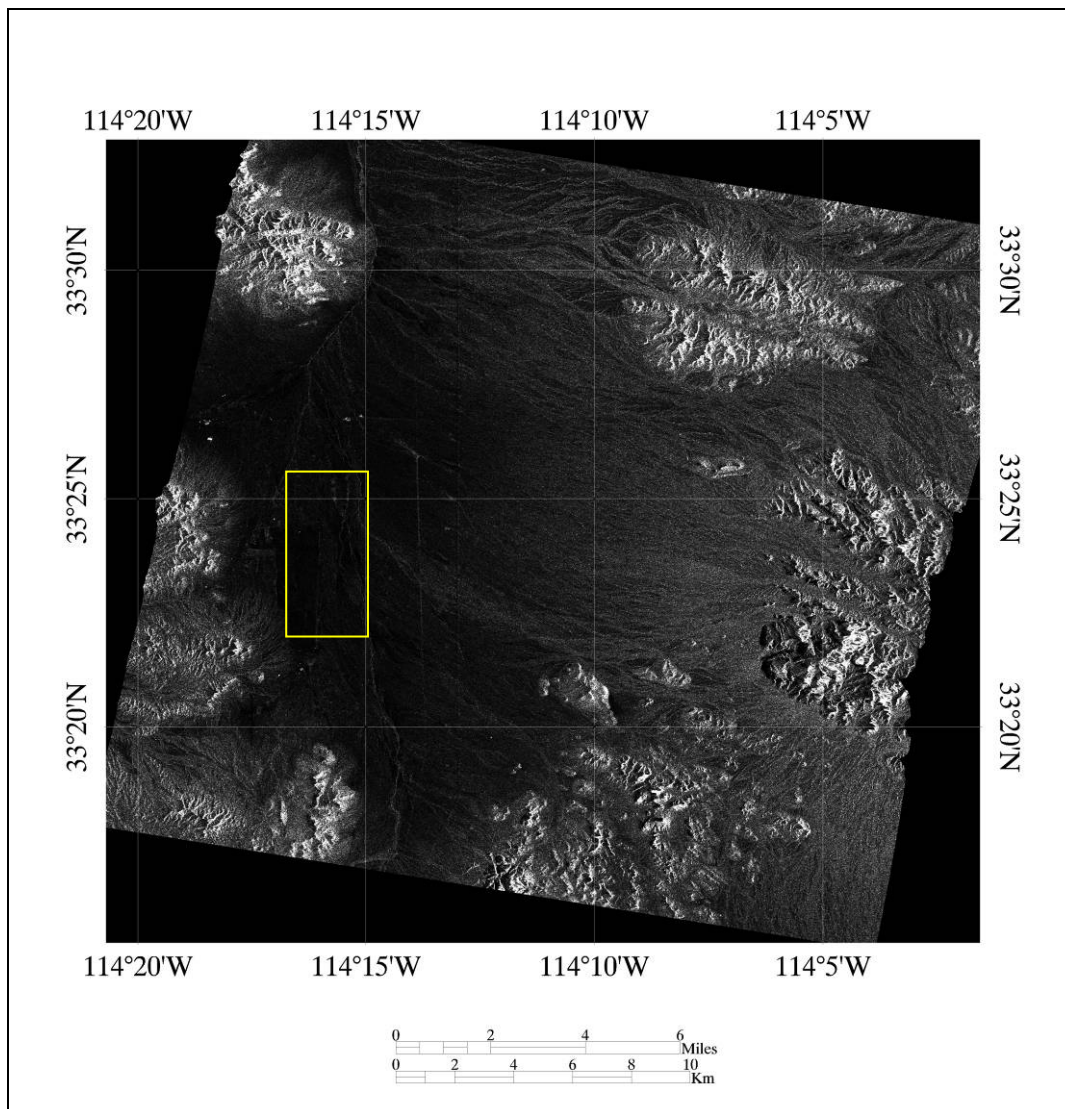


Figure 16. Georeferenced polarimetric radar image of the area of interest within Yuma Proving Ground(the yellow box denotes the brownout landing zone)

D. IMAGE TRANSFORMATION

The general approach utilized in this research was modeled after previous NPS helicopter brownout theses, specifically resampling the data to a lower resolution to average out the effects due to speckle. Speckle is responsible for the grainy appearance of radar images. Data compression is characterized by large amounts of information being compacted into fewer bands by reducing the dimensionality of the data. The radar

image file was large, so it was compressed using IDL, once by ten percent and once by twenty percent. The necessary IDL codes to compress the polarimetric radar data was written by Dr. R. C. Olsen (Appendices C and D). These IDL codes created radar images that were useful and clear to an average analyst/observer, because of the reduced effects of speckle.

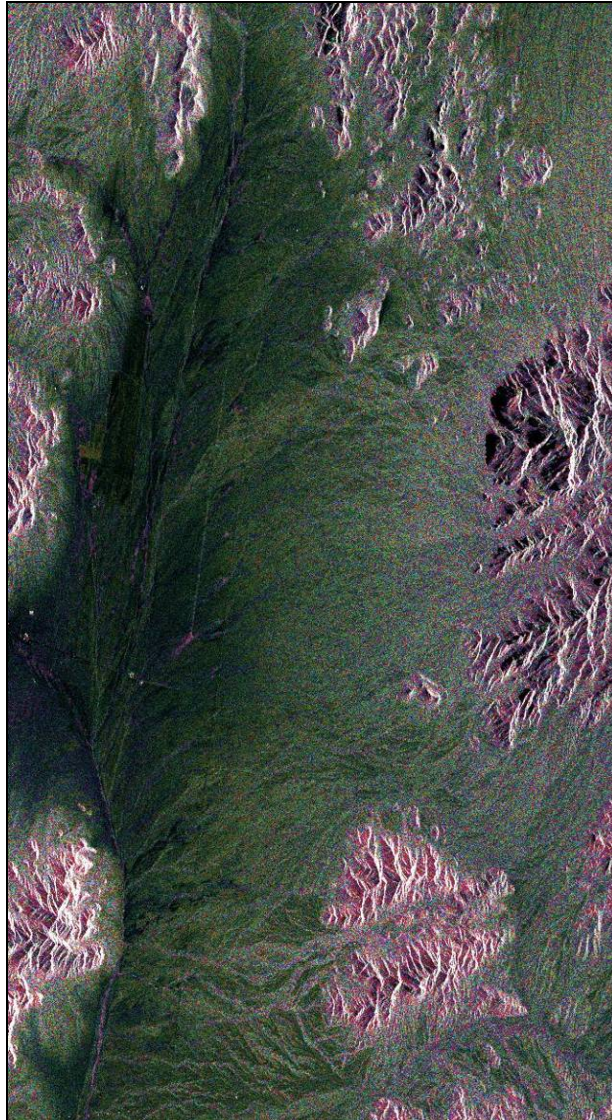


Figure 17. Twenty percent compressed polarimetric radar image of the area of interest within Yuma Proving Ground

Above is the 20 percent compressed polarimetric radar image, colorized in Red-Green-Blue (RGB), of the area of interest within Yuma Proving Ground. Figure 17 was

created by calculating the Principal Component Transform from the four-band polarimetric (real) data, at 20 percent average/reduction. The first three principal components are mapped to Hue, Lightness (or Intensity), and Saturation. The bands are then converted to the Red-Green-Blue color space and displayed.

Below is the 10 percent compressed polarimetric radar image, colorized in Red-Green-Blue (RGB), of the area of interest within Yuma Proving Ground.

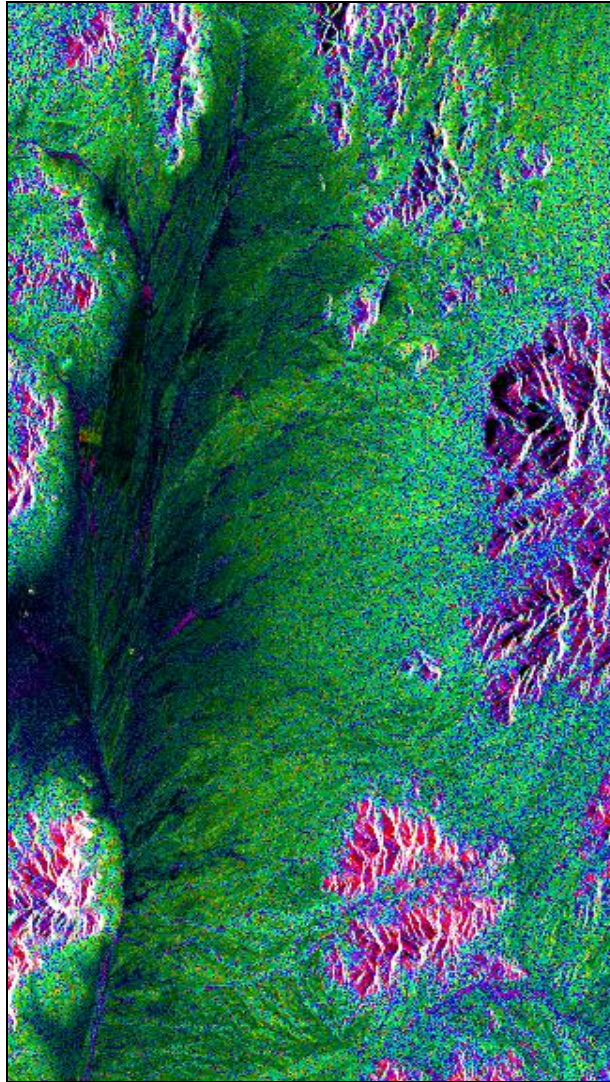


Figure 18. Ten percent compressed polarimetric radar image of the area of interest within Yuma Proving Ground

Figure 18 was created by, in sequence, reducing/averaging the polarimetric data to one-tenth the size of the original file (10:1 reduction), then taking the principal

component transform, then mapping into IHS, such that PC1 is Intensity, PC2 is Hue, PC3 is Saturation. In this illustration, saturation has been set to one for all pixels. With mapping complete, the image is inverted from the IHS color space (or alternately Hue-Lightness-Saturation) to the Red-Green-Blue (RGB) coordinate system.

Once the image data files were loaded into ENVI, they were manipulated for processing using visualization and statistical methods.

E. IDENTIFY AREAS OF INTEREST

With a more useful radar image, Areas of Interest (AOIs) were located. This was based upon prior knowledge of ground truth data of the YPG. Specifically, the research focused on the known brownout landing zone in YPG, as well as the surrounding areas known not to cause brownout. The statistics of each AOI were calculated using ENVI histograms to determine if there were any factors that could be used to distinguish brownout from non-brownout areas. It was noted that brownout areas tended to have a lower mean digital number than the non-brownout areas.

F. HISTOGRAMS

“Many image-processing techniques begin with an examination of the statistics of the scene or image; in particular, an important technique is to examine the histogram of occurrences in a scene” (Olsen, 2007, p. 142). Based on the fact that brownout areas tend to appear darker than non-brownout areas, it was determined that looking at the distribution of digital number values throughout the entire scene could be useful. Within ENVI, a histogram is a “frequency distribution calculation and gives the number of points, cumulative points, percent for each bin, and cumulative percentage for each digital number in the image histogram” (Research Systems, Inc., 2005, p. 468). Since the radar return is directly correlated to soil’s particle size distribution, surface roughness, and moisture data, there is a physical correlation between the distribution of digital number values in the image, and the occurrence of soil types in the scene.

The histogram shows the distribution of digital number values within the image, and was used to partition the imagery. The data encompassed three broad regions that defined the histogram. The code used to create histogram images is shown in Appendices A and B. The histograms are illustrated in Figures 19–22.

Figure 19 shows the histogram for the Horizontal transmit-Horizontal receive (HH) data, after compressing/averaging the data by a factor of ten to reduce speckle.

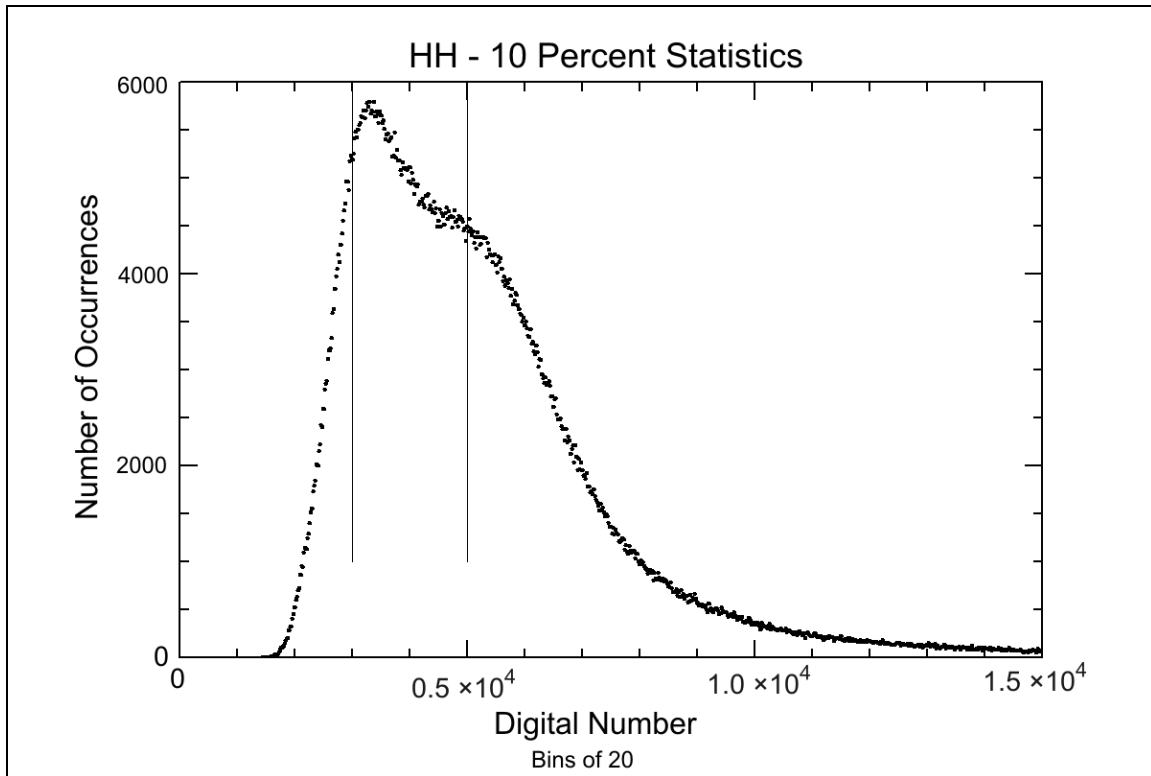


Figure 19. Illustration of the histogram using ten percent polarimetric radar data in the Horizontal transmit-Horizontal receive (HH) mode

In this HH mode, what was observed was a distinctive shape that looked like the sum of two Gaussian distributions. The analysis approach described below uses thresholds at digital number values of 3000 and 5000; these values are denoted by the vertical lines.

Figure 20 shows the histogram distribution for the Vertical transmit-Vertical receive (VV) mode, again reduced by a factor of ten to remove speckle.

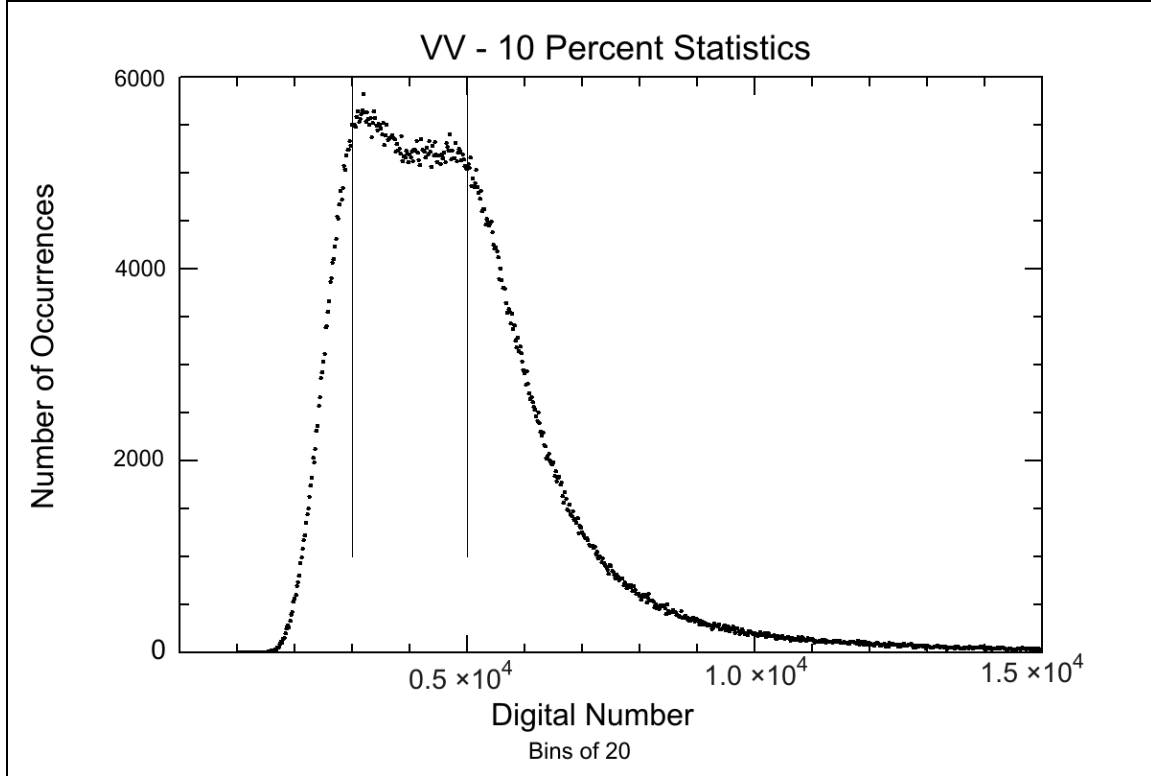


Figure 20. Illustration of the histogram using ten percent polarimetric radar data in the Vertical transmit-Vertical receive (VV) mode

The VV mode distribution again appears to be the sum of two distributions, with a local minimum (or break) at a digital number value of 4000. Since large samples drawn randomly from natural populations usually produce a symmetrical frequency distribution, these predictable bell-shaped curves were observed for these two modes.

Finally, Figure 21 shows the histogram distribution for the cross-polarized radar data, specifically in the Vertical transmit-Horizontal receive (VH) mode. Here, there appears to be only one random distribution of returns, with considerably lower digital number values.

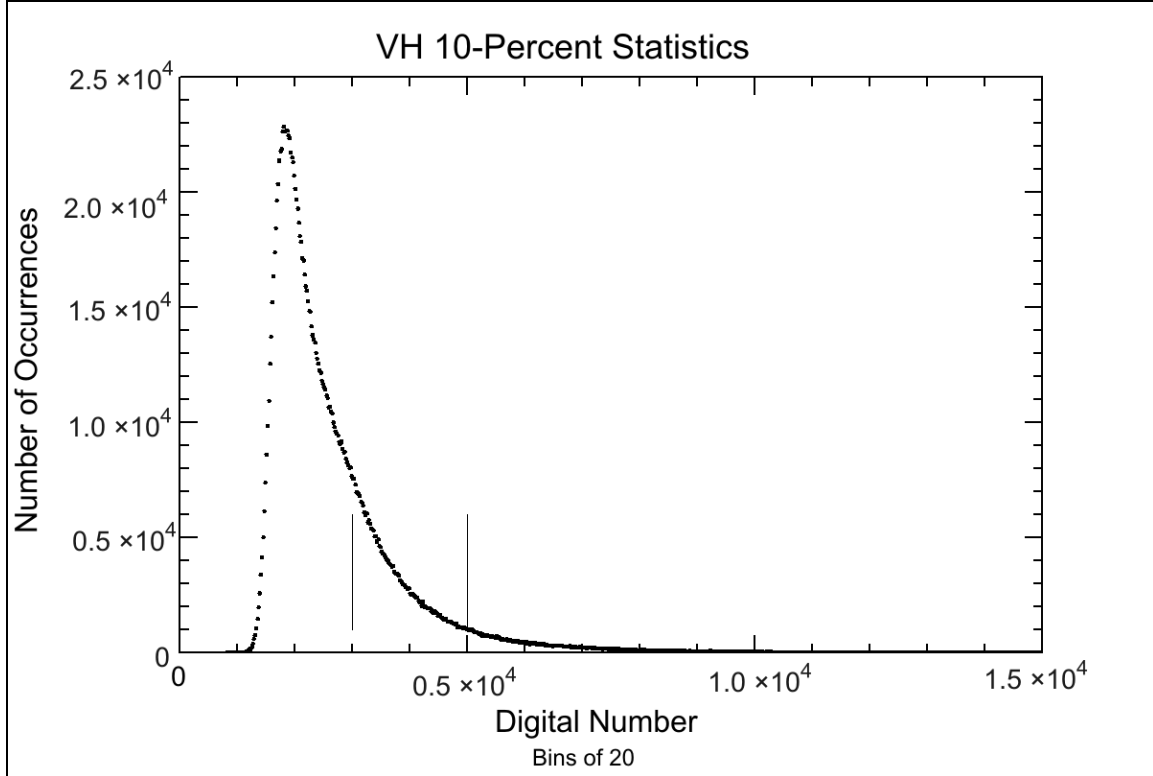


Figure 21. Illustration of the histogram using ten percent polarimetric radar data in the Vertical transmit-Horizontal receive (VH) mode

Both the HV and VH histograms were positively skewed, having less digital numbers, both in totality of digital numbers and in number of occurrences per digital number. Of particular note, the values in the 3000 to 5000 digital number range were considerably lower (denoted by the vertical lines).

Further comparison of the VV and HH returns is illustrated in Figure 22. The histogram illustration showed the ten percent compressed polarimetric radar data in the Horizontal transmit-Horizontal receive (HH) mode combined with the Vertical transmit-Vertical receive (VV) mode. This illustrates the relatively higher returns in the second peak between digital number values of 4000-5000 in the VV vice HH. This difference would be helpful in distinguishing natural phenomena, but is less important for the purpose of this research (brownout).

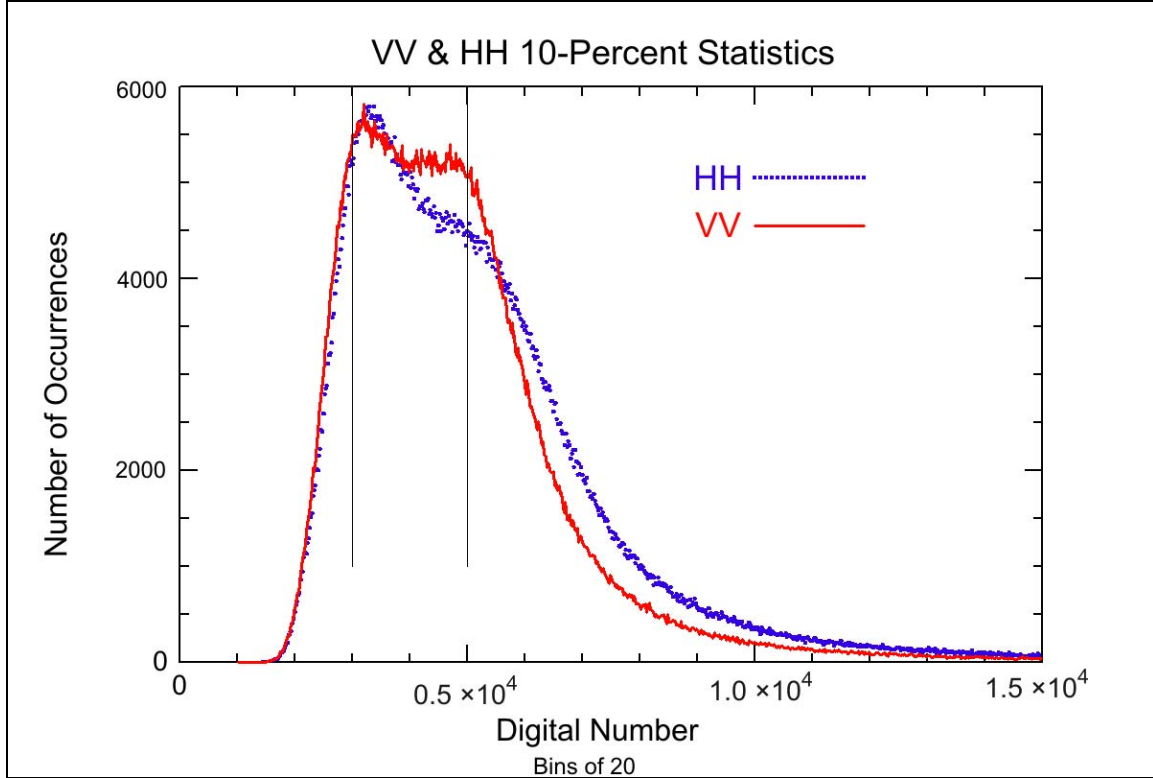


Figure 22. Illustration of the histogram using ten percent polarimetric radar data in the Horizontal transmit-Horizontal receive (HH) mode (colored in blue) combined with the Vertical transmit-Vertical receive (VV) mode (colored in red)

G. PARTITION BY DIGITAL NUMBERS

Following a model established in previous thesis work at NPS, the darker brownout region (lower digital numbers and radar returns) is distinguished from good landing zones by thresholding the data. Using the histograms, thresholds were chosen to be used in the Density Slice function. The values are as follows:

Minimum Value	Maximum Value	Color
0	3000	Red
3001	5000	Sienna
5001	image default max	Green

Table 2. Threshold Values.

The rationale was to use digital numbers to determine relative values for different land cover delineation. Using the information gleaned from the histograms, it was determined that the digital numbers could be partitioned into three ranges, which would delineate brownout (low digital number and dark radar return), ambiguous (due to break histogram), and non-brownout areas (higher digital number and bright radar return).

H. DENSITY SLICE

ENVI provides a **Class Color Mapping** function, which allows the user to preselect a color that corresponds to an area of interest for an unsupervised classification. For this research, the interactive Density Slice function was utilized to manually select data ranges and colors, which highlighted areas of interest in the grayscale image. This was accomplished by selecting **Tools → Color Mapping → Density Slice**. After clearing the default ranges, the three partitioned ranges were then manually entered by selecting **Options → Add New Ranges**.

The default colors for the partitioned ranges were also changed to those shown in Table 2. The data ranges were identified using the histograms, which ensured the brownout susceptible regions could be easily identified (Table 2). Once the Density Slice function was executed, the colors were applied to the uncompressed grayscale radar image in VV polarization mode.

The grayscale polarimetric radar image of Yuma Proving Grounds is seen in Figure 23. Landing Zone 1 is delineated by the yellow box.

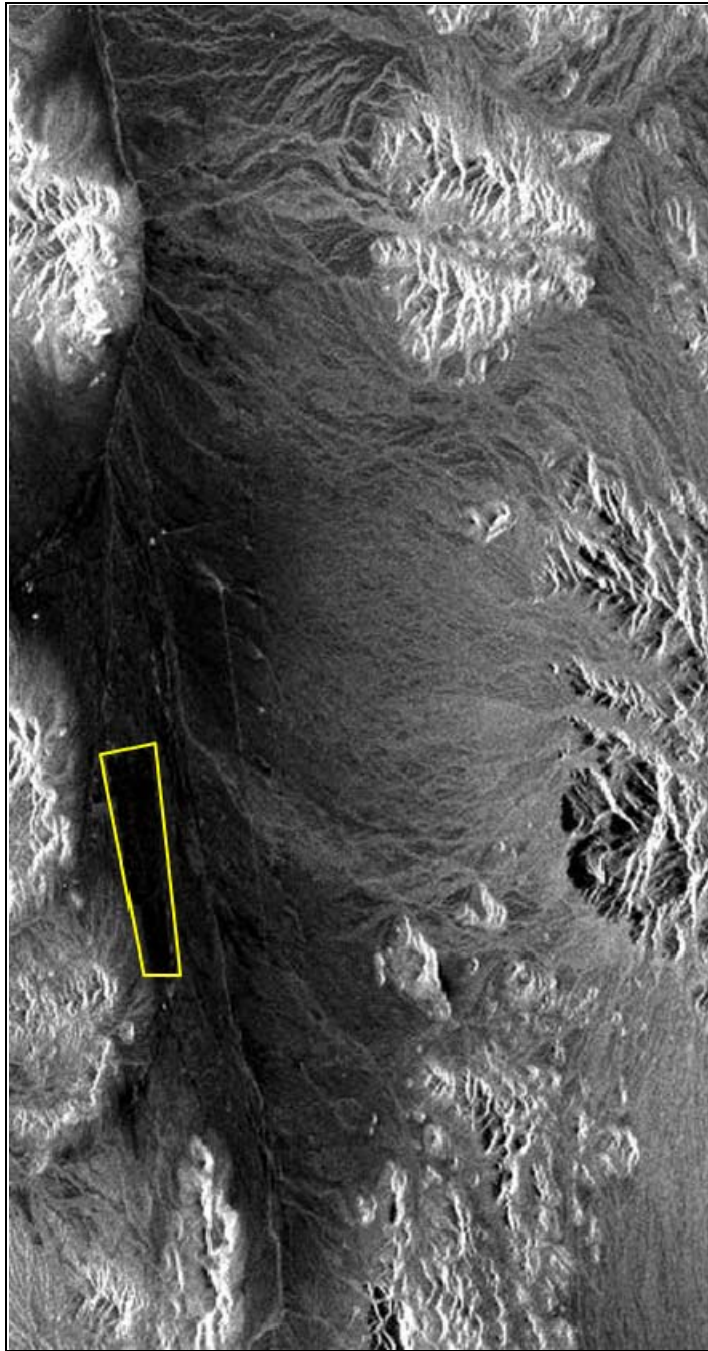


Figure 23. Grayscale of polarimetric radar image (VV polarization)

The polarimetric radar image after the Brownout Algorithm is applied in Figure 24. Landing Zone 1 is delineated by the blue box.

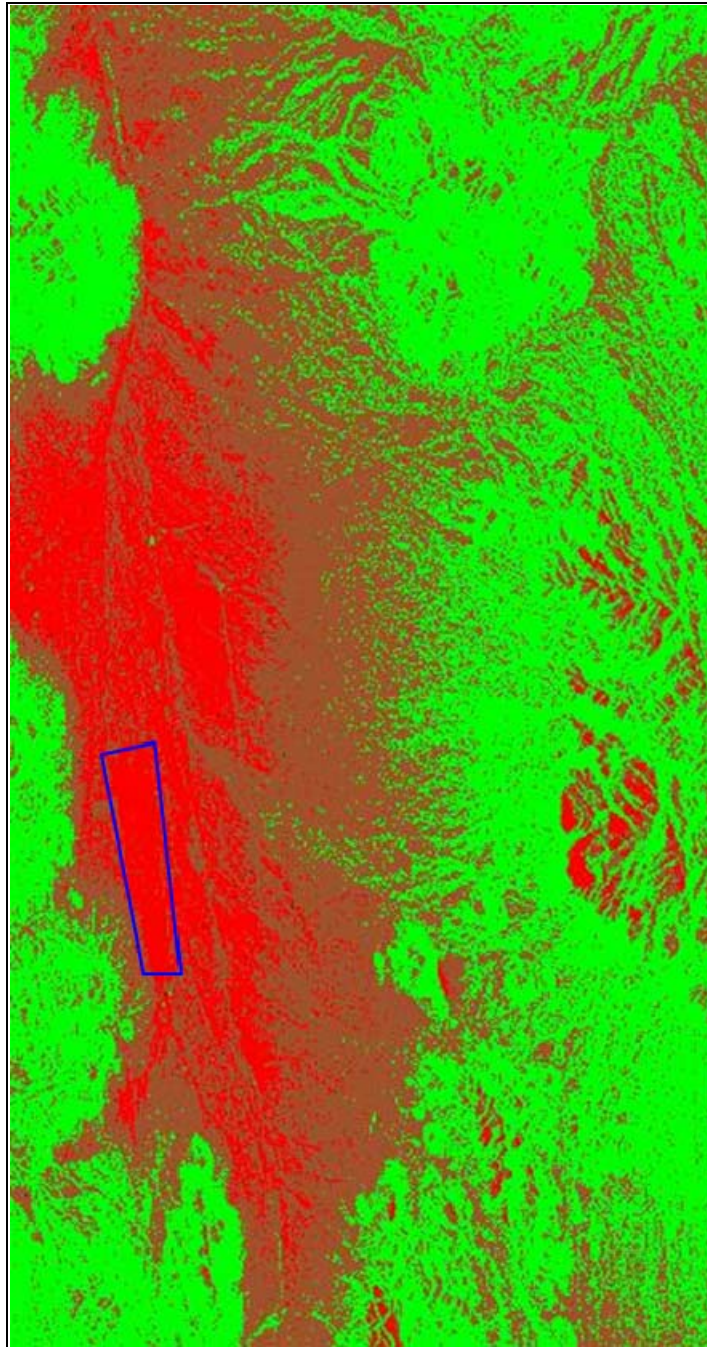


Figure 24. Polarimetric radar image after Brownout Algorithm is applied

Based on field work, and much previous experience in the analysis of data from this region, it is apparent that the brownout zone is well identified by this process. Unfortunately, the resulting spatial resolution of this product is a little low, and direct quantitative evaluation is not practical. (The area has been enlarged and altered in the time between the radar observations and this work.)

I. BROWNOUT ALGORITHM

The Brownout Algorithm is therefore directly associated with the Density Slice function, and these partitions were applied to the polarimetric radar data to show, by color, which areas provide a safe landing environment and those that do not. Having discovered that the three ranges of digital number values appeared to correspond to the soil characteristics, the Brownout Algorithm was then applied, and the results examined.

J. RESULTS

As anticipated, the cross-polarized signals (VH and HV) had weaker radar backscatter intensity than the like-polarized signals (VV and HH). This is shown by the positive skewing of the histograms for VH and HV as well as a lower number of occurrences of digital number, as well as, a lower overall bins of digital numbers.

Focusing on those aspects that were central to polarimetric radar, soil texture (i.e., smaller size appears darker), surface roughness (i.e., darker implies smoother), and the dielectric constant (i.e., the wetter the soil, the higher and brighter the radar return), the analysis of the histograms was conducted. Recall that the soil within Landing Zone 1 of YPG is smooth, dry sand that is conducive to brownout conditions. This soil appeared dark on the polarimetric image and had a corresponding low value for a digital number. It was assumed that similar soils would appear the same. Conversely, a bright return and a subsequent higher value of digital number would imply that either the soil was dissimilar to that of Landing Zone 1, or had some degree of moisture content, and was less likely to produce brownout conditions.

Since the radiations scattered from soil depend upon its dielectric constant, surface roughness, and state of polarization, according to Gupta and Jangid (2008, p.

885), it follows that there would be differences between the cross-polarized data and the co-polarized data, as well as the difference in the amount of return. Further analysis was completed to explore the relationships between the different polarizations, and to include possible differences in the non-brownout areas (the regions with digital number values between 3000 and 4000 in HH and VV).

K. IN-DEPTH ANALYSIS

The distinctive break shown previously in the histogram for the HH and VV polarizations (Figure 22) appeared to have its low point at digital number of approximately 4000. Visual analysis of these results warranted further examination. The colors are associated with the updated threshold values became:

Minimum Value	Maximum Value	Color
0	3000	Red
3001	4000	Sienna
4001	5000	Yellow
5001	image default max	Green

Table 3. Updated threshold values

Figure 25 is a two-dimensional scatter plot created in ENVI, which shows a strong positive correlation between the two co-polarizations. Regions of interest were created by applying the thresholds values of 3000, 4000 and 5000 to the VV polarization radar image. The scatter plot of VV versus HH digital number values for these regions of interest shows the positive correlation between the two polarizations, because the data points are clustered along a trend line with an upward slope, meaning as one variable increases so does the other.

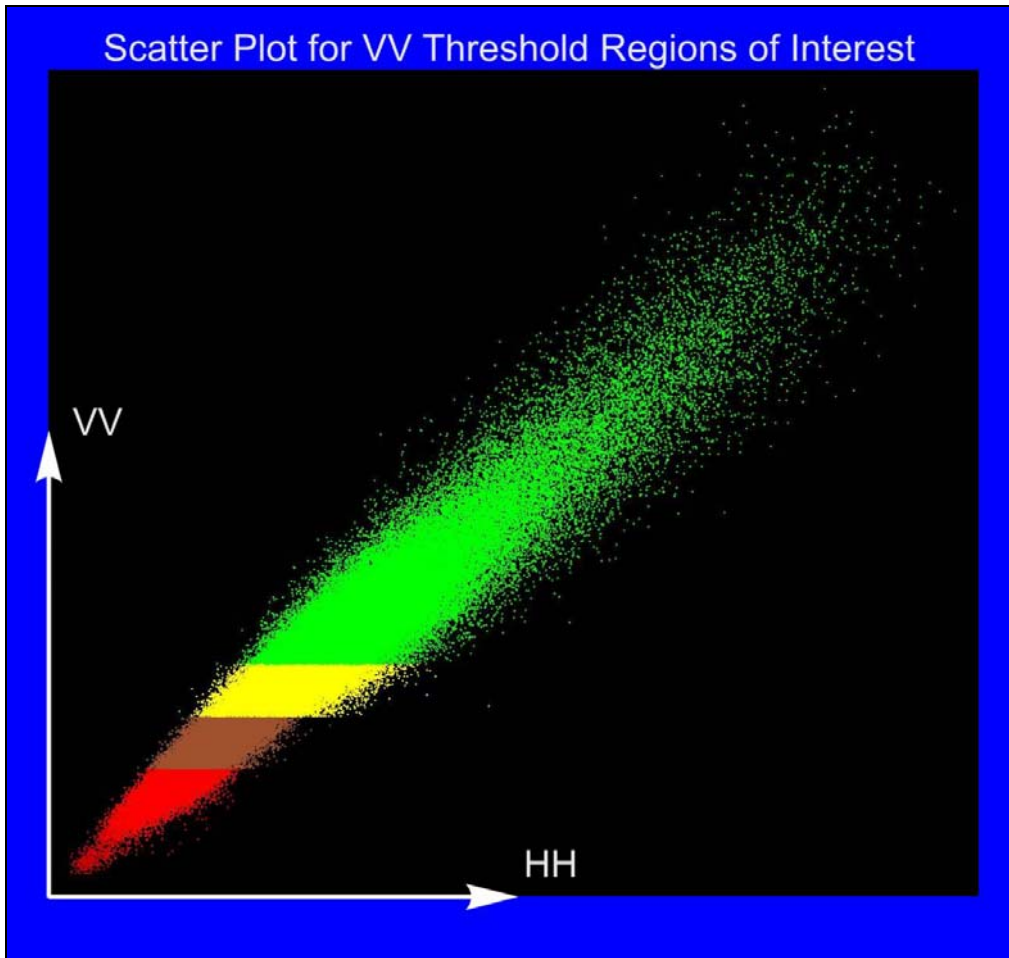


Figure 25. Scatter plot comparing VV polarization to HH polarization which shows the VV thresholds (breaks at 3000, 4000, and 5000)

A second scatter plot using the same regions of interest was created to illustrate the degree of correlation between the HH and HV polarizations (Figure 26). As compared to the co-polarization scatter plot shown in Figure 25, the demarcations between the regions of interest are less defined.

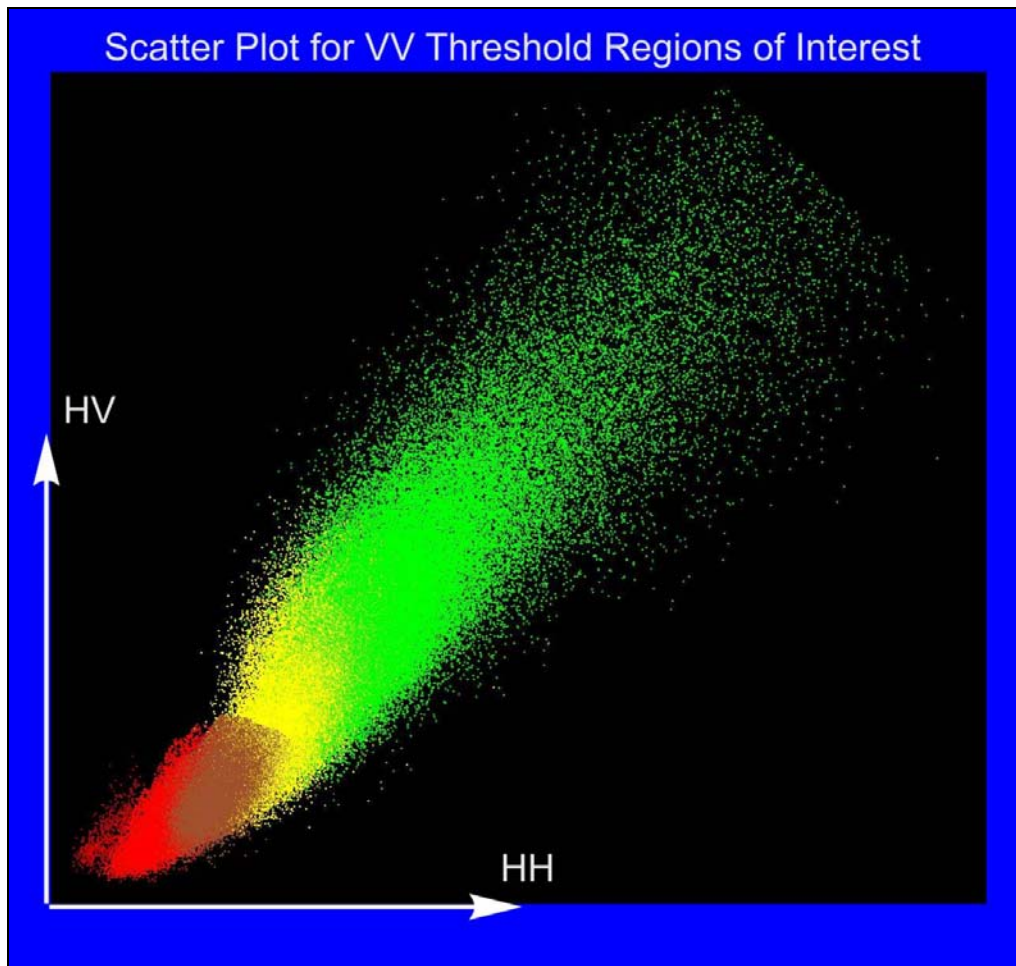


Figure 26. Scatter plot comparing HH polarization to HV polarization which shows the VV thresholds (breaks at 3000, 4000, and 5000)

These new threshold values were updated into the brownout algorithm to produce a new colorized radar image (Figure 27). A similar image was produced, but with a more clarifying outcome. Echoing the aspects that were central to this research with respect to polarimetric radar and soil characteristics, Landing Zone 1 was anticipated to appear red due to the corresponding low digital number value caused by smooth, dry sand that is conducive to brownout conditions. Once more, it was expected that similar soils would appear the same, and that a bright return with a higher digital number value would mean that either the soil was different to that of Landing Zone 1, or had some degree of moisture content, and was less likely to produce brownout conditions.

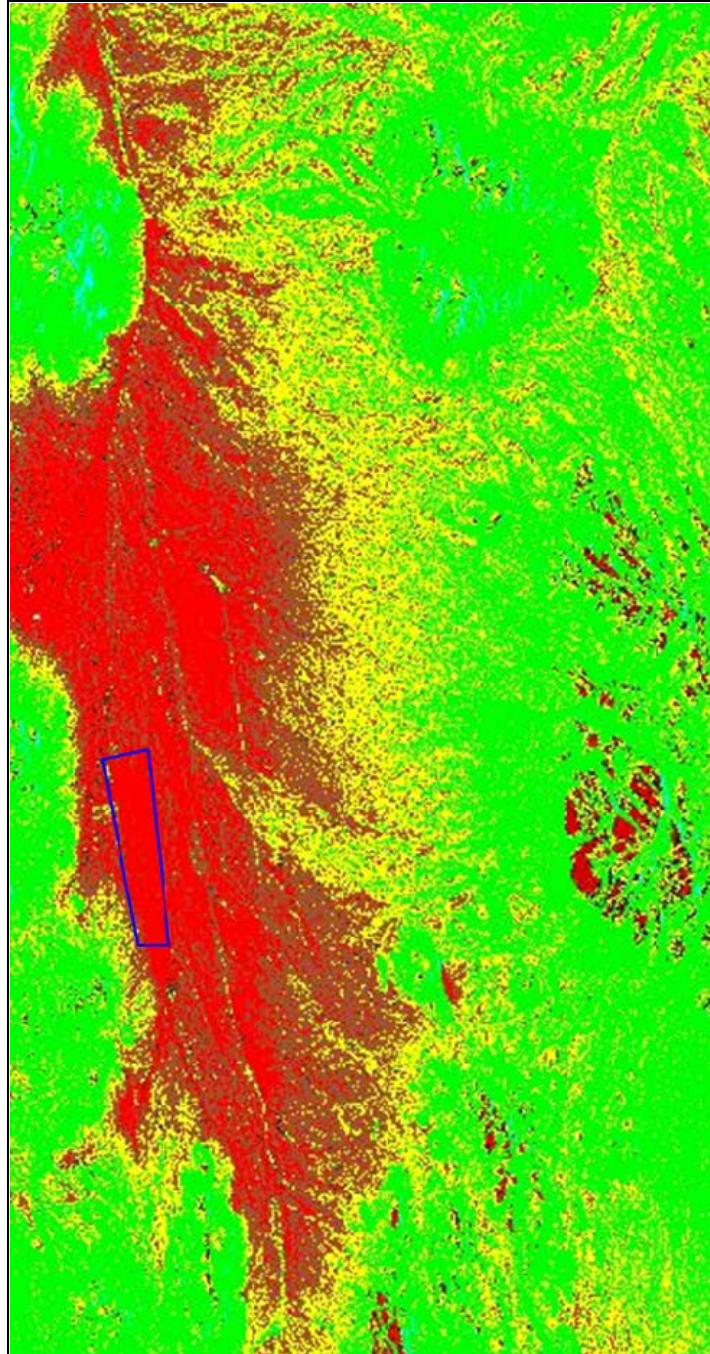


Figure 27. Polarimetric radar image (VV polarization) after new Brownout Algorithm threshold values are applied (Landing Zone 1 denoted by blue box)

As before, it was worthwhile to view the histograms of the radar image. The histogram for the HH polarization for the four regions is illustrated in Figure 28.

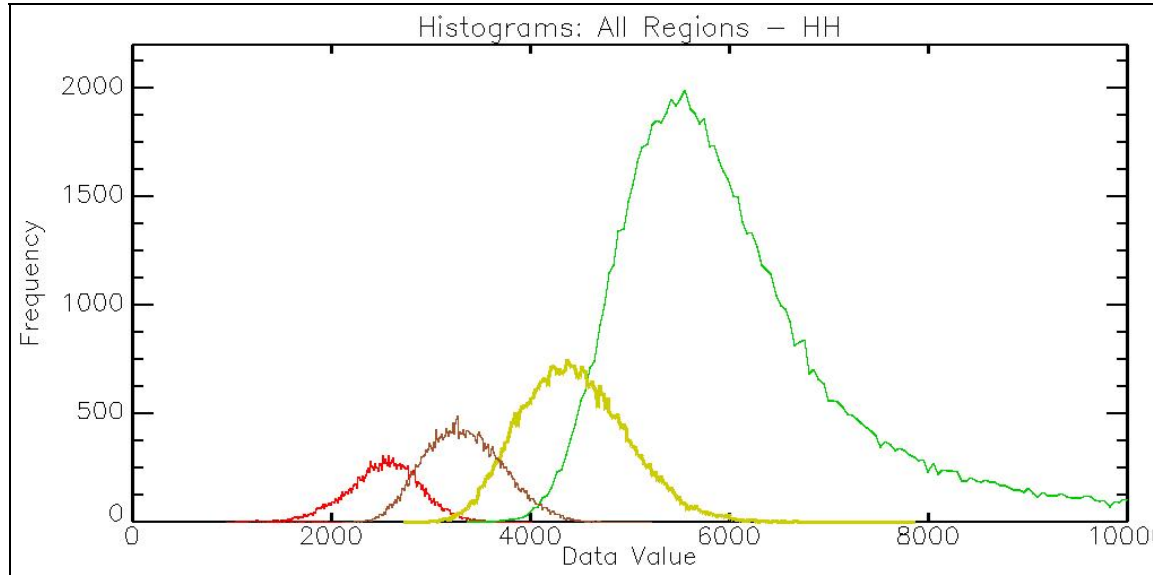


Figure 28. Histogram of the red, sienna, yellow, and green regions of the brownout algorithm using the HH polarization (there is also a dark component with very low frequency and low digital number not visible on this scale)

The red region of interest (essentially the brownout region) shows a reasonably narrow range of digital numbers, reflecting the high correlation between VV and HH—these digital number values are all below 3000 in VV. Similarly, the sienna region reflects the digital number range of 3000–4000 in VV. The distribution of HH values for the yellow region of interest corresponds to VV values of 4000–5000, while the green curve corresponds to VV values over 5000.

Figure 29 shows the means for the VV selected regions in each polarization band. As one might expect, the VV and HH means are very similar, while the cross-polarized components are much lower. These indicate a possible path for more sophisticated supervised classification approaches that would use the multi-band information, but it should be noted that a number of attempts to do so within this research were not particularly successful.

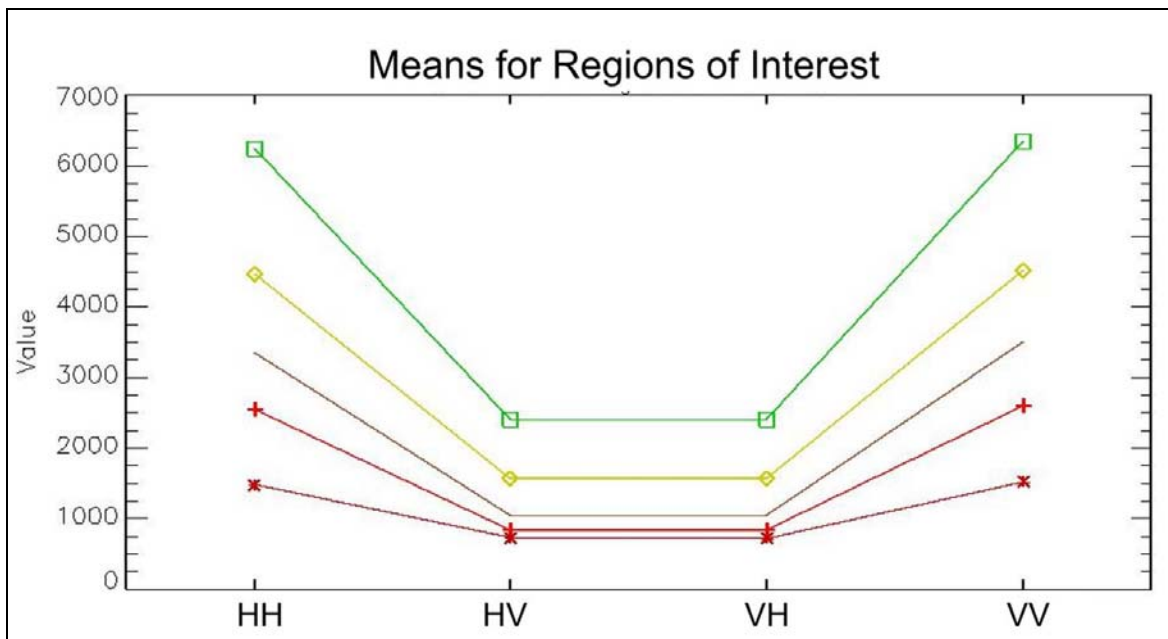


Figure 29. Mean values for each region of interest by polarization

Because of the differences between the regions of interest, it appeared to be worthwhile to analyze the red, yellow, and green regions individually, expressly by creating their own histograms using the quadrature polarizations (Figures 30–32). Of particular note is the change in values concerning the VV polarization between each of the regions of interest.

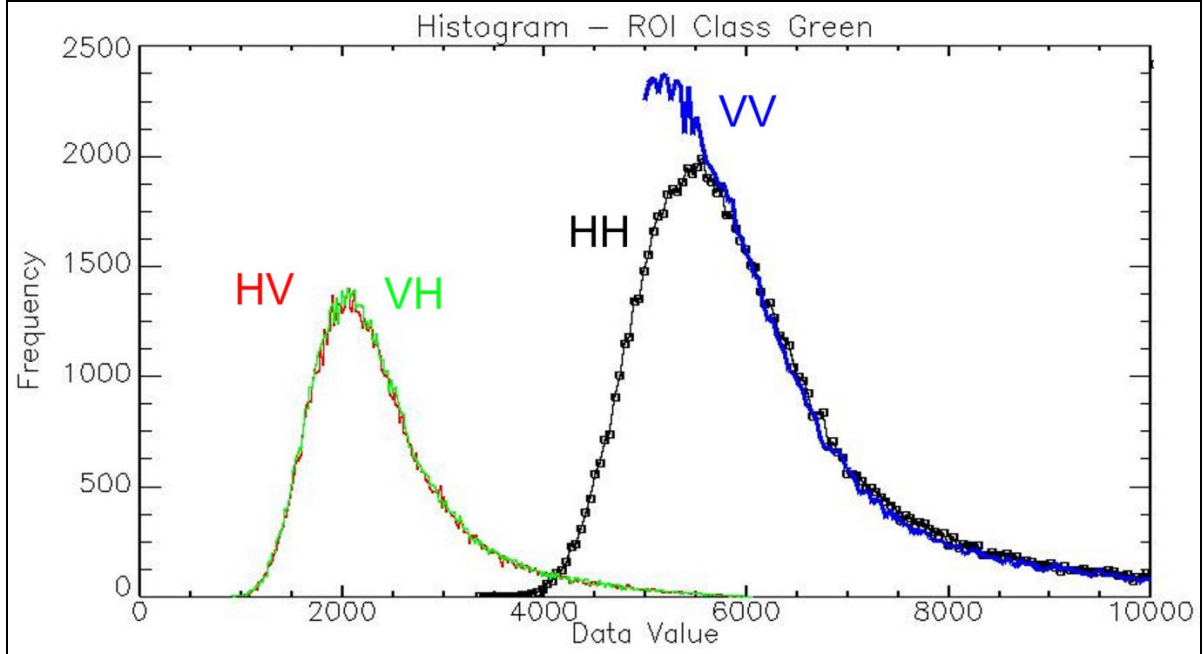


Figure 30. Histogram of the green region of interest for all four polarizations using the region defined by VV values greater than 5000

Figure 30 shows the histogram for the “green” region of interest, a region defined by the VV polarization values greater than 5000. The green region of interest showed that the cross-polarization had a lower radar return (low digital number values), while the co-polarization components (VV, HH) both had high values near 6000.

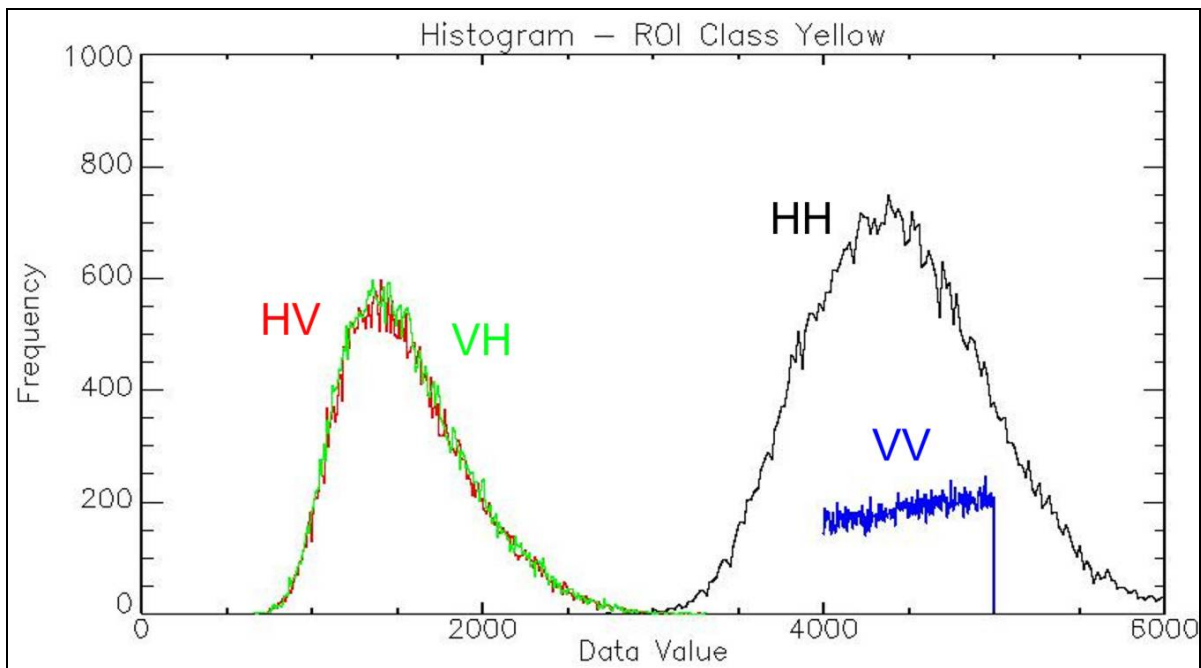


Figure 31. Histogram of the yellow region of interest for all four polarizations using the region defined by VV values from 4000–5000

Figure 31 shows the histogram for the four returns as defined in the “yellow” region of interest. This region is defined by the VV polarization values between 4000 and 5000. The yellow region was similar to the green region values in the cross-polarization and HH but was found to have a distinctly lower value in frequency for the VV polarization.

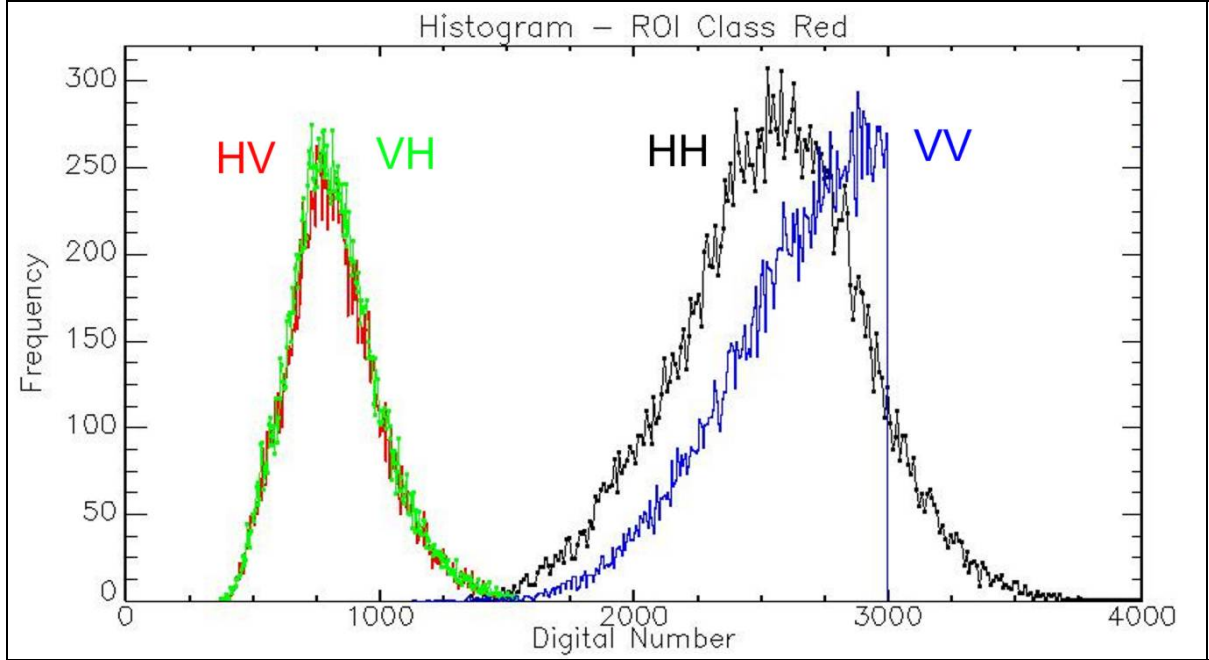


Figure 32. Histogram of the red region of interest for all four polarizations using the region defined by VV values less than 3000

Figure 32 shows the histogram distributions for the “red” region of interest, which is the region defined by the VV polarization values less than 3000. By comparison to Figure 30, the HH and VV peaks are interchanged and is likely to be a characterization that could be utilized to determine the brownout regions. The offsets in the peaks of the HH and VV polarizations in these distributions again reflect the possibility of extracting useful information from the different polarizations. Unfortunately, this was outside the scope of this research to explore this further.

THIS PAGE INTENTIONALLY LEFT BLANK

V. CONCLUSION

The overall results of this research represented by the analysis in Chapter IV were interesting and encouraging. The attempt to characterize meaningful intelligence about the soils types by analyzing polarimetric radar for intensity appears to be a viable solution for the detection of and therefore the avoidance of brownout conditions.

Polarimetric radar appears to have a wider utility than anticipated, particularly with respect to soil characterization. Military operations continue to be in diverse environments, relying heavily on remote sensing techniques to provide necessary information for planning. While soils may vary by location, climate, and physical properties, prior knowledge of those soils via remote sensing can provide mission planners with the information needed to make improved operational risk assessments. This is especially true with respect to helicopter brownout. With the all-weather capability, polarization effects, and soil characterizations, radar and microwave energy can be effectively utilized to predict helicopter brownout.

While the best way to handle brownout conditions is to avoid them altogether, the mission may dictate the landing zone selection. The fundamental objective of this thesis was to examine the ability to remotely predict helicopter brownout conditions using polarimetric radar. An analysis of soil characteristics, particularly soil moisture content, particle size distribution, and surface texture yielded positive results. The author hopes this algorithm can be used to predict and therefore prevent helicopter brownout mishaps.

THIS PAGE INTENTIONALLY LEFT BLANK

VI. CONSIDERATIONS FOR FOLLOW-ON ACTIVITIES

A. GENERAL RECOMMENDATIONS

1. Applications

There are several flight tools that can be used often for military flight mission planning. Application of this brownout algorithm within such tools could have beneficial effects, such as ‘Falcon View’ for real time changes or ‘Top Scene’ for preflight planning. Outside the military, a general utilization with an imaging system/human observers’ imaging application in order to characterize soil properties could also have positive results.

2. Validation

While the outcome of this research was illuminating, there still exists the need to validate the results, and to refine the values. This could include the following:

- 1) Explore how the geometry of SAR can affect the results, such as geometry distortions and azimuth ambiguity.
- 2) Conduct studies about depth of loose topsoil versus surface crusting.
- 3) Conduct more detailed soil studies, concentrating on other properties of soils.
- 4) Evaluate what causes the co-polarized break in the histogram.

THIS PAGE INTENTIONALLY LEFT BLANK

APPENDIX A. IDL CODES FOR INDIVIDUAL HISTOGRAMS

The following text is the IDL code written by Dr. R. C. Olsen of the Naval Postgraduate School Remote Sensing Center to create individual histograms from the polarimetric radar data (Figures 19-21).

```
factor = 20
hist = histogram(data/factor, omin = mini, omax = maxi)
nele = n_elements(hist)

xh = findgen(nele)+ mini
window, 1, xsize = 1200, ysize = 800
RADIUS = .4
circle = 2*!pi*findgen(9)/8
usersym, radius*sin(circle), radius*cos(circle), /fill
plot, xh*factor, hist, psym = 8, xrange = [0, 1.5e4], xstyle = 1, $
xticks = 3, xminor = 5, title = 'HH 10 Percent Statistics', $
xtitle = 'Digital Number', ytitle = 'Number of Occurrence', $
subtitle = '!DBins of 20!N ', charsize = 1.1, $
pos = [0.15, 0.15, 0.9, 0.9], /normal, xthick = 2, ythick = 2, $
xtickname = [' ', ' ', ' ', ' '], xticklen = 0.03

plots, [1,1]*3e3, [1000, 6000], linestyle=0
plots, [1,1]*5e3, [1000, 6000], linestyle=0

image = tvrd()
image = 255b- image
dir = "O:\S_Students\RABAJA\Olsens_work\"
file = 'Histogram_HH_10pct.png'
write_png, dir + file, image

end
```

THIS PAGE INTENTIONALLY LEFT BLANK

APPENDIX B. IDL CODES FOR COMBINED HISTOGRAM

The following text is the IDL code written by Dr. R. C. Olsen of the Naval Postgraduate School Remote Sensing Center to create a combined histogram from the polarimetric radar data (Figure 22).

```
factor = 20
hh_hist = histogram(hh_data/factor, omin = mini, omax = maxi)
nele = n_elements(hh_hist)
xhh = findgen(nele)+ mini

vv_hist = histogram(vv_data/factor, omin = mini, omax = maxi)
nele = n_elements(vv_hist)
xvv = findgen(nele)+ mini

hh_color = 50

window, 1, xsize = 1200, ysize = 800
device, decomposed = 0
loadct, 13
tvlct, r,g ,b, /get
r(255) = 255
g(255) = 255
b(255) = 255
r(0) = 0
g(0) = 0
b(0) = 0
tvlct, r, g, b

RAdius = .4
circle = 2*!pi*findgen(9)/8
usersym, radius*sin(circle), radius*cos(circle), /fill
erase, 255
plot, xhh*factor, hh_hist, psym = 8, xrange = [0, 1.5e4], xstyle = 1, $
xticks = 3, xminor = 5, title = 'HH & VV 10 Percent Statistics', $
xtitle = 'Digital Number', ytitle = 'Number of Occurence', $
subtitle = '!DBins of 20!N ', charsize = 1.1, $
pos = [0.15, 0.15, 0.9, 0.9], /normal, xthick = 2, ythick = 2, $
xtickname = [' ', ' ', ' ', ' '], xticklen = 0.03, /nodata, /noerase, color = 0

oplot, xhh*factor, hh_hist, psym = 8, color = hh_color
```

```
oplot, xvv*factor, vv_hist, psym = 0, color = 254, thick = 3
```

```
xyouts, 9e3, 5000, 'HH', color = hh_color, size = 1.4
```

```
xyouts, 9e3, 4500, 'VV', color = 254, size = 1.4
```

```
tmpx = findgen(20)*100+1e4
```

```
tmpy = tmpx & tmpy(*) = 5000
```

```
oplot, tmpx, tmpy+50, color = hh_color, psym = 8
```

```
tmpy = tmpx & tmpy(*) = 4500
```

```
oplot, tmpx, tmpy+50, color = 254, psym = 0, thick = 3
```

```
plots, [1,1]*3e3, [1000, 6000], linestyle=0, color = 1
```

```
plots, [1,1]*5e3, [1000, 6000], linestyle=0, color = 1
```

```
image = tvrd(true=1)
```

```
dir = "O:\S_Students\RABAJA\Olsens_work\"
```

```
file = 'Histogram_HH_VV_10pct.png'
```

```
write_png, dir + file, image
```

```
end
```

APPENDIX C. IDL CODES FOR TWENTY PERCENT IMAGE

The following text is the IDL code written by Dr. R. C. Olsen of the Naval Postgraduate School Remote Sensing Center to create a compressed image (by 20 percent) from the polarimetric radar data (Figure 17).

```
samples = 650
lines   = 1242
bands   = 4
;header offset = 0
;file type = ENVI Standard
;data type = 4
;interleave = bsq
;sensor type = Unknown
;byte order = 0
;default bands = { 1,2,4}
;wavelength units = Unknown
;band names = { HH, HV, VH, VV }

data = fltarr(samples, lines, bands)
file = 'ypg_20pct_pc_covar.dat'
dir   = 'C:\Documents and Settings\Rabaja\My
Documents\Radarsat_2_YPG\RS2_OK2094_PK24935_DK26063_FQ14_20080822_133
951_HH_VV_HV_VH_SLC\ypg_quad_pol_10pct\PC\'
dir   = 'C:\Documents and Settings\Rabaja\My
Documents\Radarsat_2_YPG\RS2_OK2094_PK24935_DK26063_FQ14_20080822_133
951_HH_VV_HV_VH_SLC\ypg_quad_pol_20pct\PC\'

cd, dir
openr, 1, file
forrd, 1, data
close, 1

; scale for HLS
;Hue Lightness Saturation (double cone). Also known as HSL and HSI.
;Hue is measured in degrees between 0 and 360, with 0 corresponding to red, 120 to
green, and 240 to blue.
;Lightness and Saturation are floating-point values between 0 and 1.

; pc1 is intensity
; pc2 is hue
; pc3 is saturation
```

```

image_in = data(*,*,0)
pct = 1.
scale = 1
pct_stretch, image_in,pct,min_val,max_val,scale=scale
help, min_val, max_val
real_min = min(image_in) & real_max = max (image_in)

mini = (real_min + min_val)/2.
maxi = (real_max + max_val)/2.
maxi = max_val
delta = maxi - mini
help, delta, real_max- real_min
intensity = ( image_in - mini) /delta
index = where ( intensity lt 0)
index2 = where ( intensity gt 1)
intensity (index) = 0
intensity (index2) = 1

window, 1, title = 'PC1'
plot, histogram ( intensity * 100.), xstyle = 1, xrange = [0, 100]
wshow
wait, 1
;;;;;;;;;;
print, 'principal component 2'
window, 2, title = 'PC2'
image_in = data(*,*,1)
real_min = min(image_in) & real_max = max (image_in)
print, real_min, real_max
H2 = histogram (image_in)
nele = n_elements (h2) & x2 = indgen(nele) + real_min & print, nele
window, 0
wset, 0
plot, x2, h2, title = 'pc2 HISTOGRAM' ; & stop
pct = 0.1
scale = 1.
wset, 2
pct_stretch, image_in,pct,min_val,max_val,scale=scale
help, min_val, max_val

mini = (real_min + min_val)/2.
maxi = (real_max + max_val)/2.
;maxi = max_val
mini = real_max

```

```

MAXI = real_min
mini = min_val
maxi = max_val
mini = -1000.
maxi = 1000.
delta = maxi - mini
help, delta
hue = 360.*( image_in - mini) /delta

index = where ( hue lt 0)
index2 = where ( hue gt 360)
hue (index) = 0
hue (index2) = 360.

h22 = histogram (hue)
plot, h22, title = 'hue', xstyle = 1, xrange = [0, 360]
;,,,,,,,,,,,,,,,,,,,,,,,,,,,,,
print, 'principal component 3'
image_in = data(*,*,2)
real_min = min(image_in) & real_max = max (image_in)
print, real_min, real_max
H2 = histogram (image_in)
nele = n_elements (h2) & x2 = indgen(nele) + real_min & print, nele

;plot, x2, h2, title = 'PC3 HISTOGRAM', xrange = [-1, 1] * 2000 ; & stop
pct = 1.
scale = 1.
pct_stretch, image_in,pct,min_val,max_val,scale=scale
help, min_val, max_val

mini = (real_min + min_val)/2.
maxi = (real_max + max_val)/2.
;mini = min_val
;maxi = max_val
mini = real_max
MAXI = real_min
mini = -5000.
maxi = 5000.
delta = maxi - mini
help, mini, maxi, delta
sat = ( image_in - mini) /delta

index = where ( sat lt 0)

```

```

index2 = where ( sat gt 1, count)
sat (index) = 0
if (count gt 0) then sat (index2) = 1

window, 3
plot, histogram ( sat*100), title = 'Saturation', xstyle = 1, xrange = [0, 100]

I0 = hue
I1 = intensity
I2 = sat
;I2 (*) = 1
COLOR_CONVERT, I0, I1, I2, r, g, b , /HLS_RGB

wset, 0
tv, r
wset, 1
tv, g
wset, 2
;tv, b
wset, 3

window, 3, xsize = samples, ysize = lines
image = [ [[r]], [[g]], [[b]] ]
tv, image, true = 3

write_jpeg, 'ypg_pol_image_tyo_full.jpg', image, true = 3
end

```

APPENDIX D. IDL CODES FOR TEN PERCENT IMAGE

The following text is the IDL code written by Dr. R. C. Olsen of the Naval Postgraduate School Remote Sensing Center to create a compressed image (by 10 percent) from the polarimetric radar data (Figure 18).

```
samples = 325
lines   = 621
bands   = 4
;header offset = 0
;file type = ENVI Standard
;data type = 4
;interleave = bsq
;sensor type = Unknown
;byte order = 0
;default bands = { 1,2,4}
;wavelength units = Unknown
;band names = { HH, HV, VH, VV }

data = fltarr(samples, lines, bands)
file = 'Absolute_value_10_pct.dat'
dir   = 'C:\Documents          and          Settings\Rabaja\My
Documents\Radarsat_2_YPG\RS2_OK2094_PK24935_DK26063_FQ14_20080822_133
951_HH_VV_HV_VH_SLC\ypg_quad_pol_10pct\'
cd, dir
openr, 1, file
forrd, 1, data
close, 1

; scale for HLS
;Hue Lightness Saturation (double cone). Also known as HSL and HSI.
;Hue is measured in degrees between 0 and 360, with 0 corresponding to red, 120 to
green, and 240 to blue.
;Lightness and Saturation are floating-point values between 0 and 1.

; pc1 is intensity
; pc2 is hue
; pc3 is saturation

image_in = data(*,*,0)
pct = 1.
scale = 1
```

```

pct_stretch, image_in, pct, min_val, max_val, scale=scale
help, min_val, max_val
real_min = min(image_in) & real_max = max (image_in)

mini = (real_min + min_val)/2.
maxi = (real_max + max_val)/2.
maxi = max_val
delta = maxi - mini
help, delta, real_max- real_min
intensity = ( image_in - mini) /delta

plot, histogram ( intensity * 100.), xstyle = 1, xrange = [0, 100]
wshow
wait, 1
,,,,,,,,,,,,,
image_in = data(*,*,1)
pct = 1.
scale = 2
pct_stretch, image_in, pct, min_val, max_val, scale=scale
help, min_val, max_val
real_min = min(image_in) & real_max = max (image_in)

mini = (real_min + min_val)/2.
maxi = (real_max + max_val)/2.
maxi = max_val
delta = maxi - mini
help, delta, real_max- real_min
hue = 360*( image_in - mini) /delta

plot, histogram ( hue), title = 'hue', xstyle = 1, xrange = [0, 360]

end

```

LIST OF REFERENCES

- Anthoni, J. F. (2000). Soil Erosion and Conservation – Part 2. Retrieved 15 August 2009, from <http://www.seafriends.org.nz/enviro/soil/erosion2.htm>
- Baron, P. A. & Willeke, K. (2001). *Aerosol Measurement – Principles, Techniques, and Applications* (2nd ed.). New York: John Wiley & Sons, Inc.
- Bartalis, Z, Wagner, W., Anderson, C., Bonekamp, H., Naeimi, V., and Hasenauer, S. (2008). Validation of Coarse Resolution Microwave Soil Moisture Products. *IEEE International Geoscience & Remote Sensing Symposium 2008 Proceedings* (pp. II-173 – II-176). Boston.
- Brady, N. C. & Weil, R. R. (2004). *Elements of the Nature and Properties of Soils* (2nd ed.). New Jersey: Pearson Education, Inc.
- Brownout (aviation). (28 May 2009). Retrieved 19 July 2009, from Wikipedia, The Free Encyclopedia: [http://en.wikipedia.org/wiki/Brownout_\(aviation\)](http://en.wikipedia.org/wiki/Brownout_(aviation))
- Davis, A. W. (September 2007). Naval Postgraduate School Master's Thesis. The Use of Commercial Remote Sensing in Predicting Helicopter Brownout Conditions.
- Elachi, C. and van Zyl, J. J. (2006). *Introduction to the Physics and Techniques of Remote Sensing* (2nd ed). New Jersey: John Wiley and Sons, Inc.
- Fundamentals of Remote Sensing. (25 September 2007). Retrieved 09 May 2009, from Canada Centre for Remote Sensing Web site: http://www.ccrs.nrcan.gc.ca/resource/tutor/fundam/index_e.php
- Glossary of Remote Sensing Terms. (21 November 2005). Retrieved 17 May 2009, from Canada Centre for Remote Sensing Web site: http://www.ccrs.nrcan.gc.ca/glossary/index_e.php
- Google Earth Image. (08 June 2007). Retrieved 22 September 2009, from Google Earth.
- Gupta, V. K. & Jangid, R. A. (2008) Microwave Dielectric Parameters of Soil with Water Retained at Important Moist States under Field Conditions. *International Conference on Microwave Proceedings* (pp 885-888).
- Henderson, F. M. & Lewis, A. J. (Editors) (1998). *Principles and Applications of Imaging Radar* (3rd ed., Vol. 2). New York: John Wiley & Sons, Inc
- Jensen, J. R. (2000). *Remote Sensing of the Environment: An Earth Resource Perspective*. New Jersey: Prentice Hall.

- Jennings, G. (20 February 2008). Down in the Dirt: Helicopter Brownouts [Electronic Version]. *Jane's Defence Weekly*. Retrieved 14 September 2009, from http://search.janes.com.libproxy.nps.edu/Search/documentView.do?docId=/content1/janesdata/mags/jdw/history/jdw2008/jdw35601.htm@current&pageSelected=allJanes&keyword=helicopterbrownout&backPath=http://search.janes.com/Search&Prod_Name=JDW&
- Lee, J. & Pottier, E. (2009). *Polarimetric Radar Imaging: From Basics to Applications*. Boca Raton: CRC Press.
- Makhamreh, Z. (5-6 May 2006). *Evaluation of Soil Quality and Development Stage Using Spectral Reflectance of Soils: Case Study in Eastern Mediterranean Region*. In Proceedings of the International Conference: Soil and Desertification – Integrated Research for the Sustainable Management of Soils in Drylands. Hamburg, Germany.
- Miller, T., Borchers, B., Hendrickx, J. M. H., Hong, S., Lensen, H. A., Schwering, P. B. W., & Rhebergen, J. (2002, p. 282). *Effect of Soil Moisture on Landmine Detection using Ground Penetration Radar*. In Proceedings of SPIE Vol. 4742, pp. 281-290.
- Olsen, R.C. (2007). *Remote Sensing from Air and Space*. Washington: SPIE Press.
- Photodermatology/Photobiology. (16 September 2008). Retrieved 14 August 2009, from Clinuvel Pharmaceuticals Ltd 2008 Web site: <http://photoprotection.clinuvel.com/photodermatology-photobiology>
- Radar Polarimetry. (07 February 2007). Retrieved 15 May 2009, from Canada Centre for Remote Sensing Web site: http://www.ccrs.nrcan.gc.ca/resource/tutor/polarim/index_e.php
- Radar and Stereoscopy. (25 September 2007). Retrieved 21 May 2009, from Canada Centre for Remote Sensing Web site: http://www.ccrs.nrcan.gc.ca/resource/tutor/stereo/index_e.php
- RADARSAT-2. (2008). Retrieved 20 April 2009, from MacDonald, Dettwiler and Associates Limited Web site: <http://www.radarsat2.info/about/mission.asp>
- Research Systems, Inc. (August 2005). *ENVI 4.2 User's Guide*. Boulder, Colorado: ITT Industries.
- Sabbagh, L. (03 October 2006). Flying Blind in Iraq: U.S. Helicopters Navigate Real Desert Storms [Electronic Version]. *Popular Mechanics*, 1-4. Retrieved 20 February 2009, from http://www.popularmechanics.com/technology/military_law/4199189.html

- Sandblaster program aims to reduce helicopter accidents caused by brownouts. (2009)
Retrieved 19 July 2009, from Mobile Dev & Design Web site:
http://mobiledevdesign.com/hardware_news/reduce_helicopter_accidents_0328/
- Saxon, K., Chandler, D., & Schillinger, W. (24-29 May 1999). Wind Erosion and air Quality Research in the Northwest U.S. Columbia Plateau Organization and Progress. *The 10th International Soil Conservation Organization Meeting* (pp. 766-770). USDA-ARS National Soil Erosion Research Laboratory, Washington.
- Secretary of Defense. (30 May 2007). *Zero Preventable Accidents*. Retrieved 19 July 2009, from
<https://www.denix.osd.mil/portal/page/portal/denix/shf/References/SECDEF-Zero-Preventable-Accidents.pdf>
- Skinner, T. (07 October 2008). Feeling the Strain: Helicopters Bear up to Work in Hostile Environments [Electronic Version]. *International Defence Review*. Retrieved 14 September 2009, from:
http://search.janes.com.libproxy.nps.edu/Search/documentView.do?docId=/content1/janesdata/mags/idr/history/idr2008/idr11701.htm@current&pageSelected=allJanes&keyword=helicopter+brownout+Marines&backPath=http://search.janes.com/Search&Prod_Name=IDR&
- Science and Operational Applications Research for RADARSAT-2. (11 May 2009). Retrieved 21 September 2009, from
<http://radarsat.space.gc.ca/eng/programs/soar/default.asp>
- Tyo, J. S., Pugh Jr., E. N., & Engheta, N. (February 1998). Colorimetric Representations for use with Polarization-Difference Imaging of Objects in Scattering Media. *Journal of the Optical Society of America A, Volume 15, Number 2*, pp. 367-374.
- United States Department of Agriculture, Natural Resources Conservation Service. (08 September 2008). *National Soil Survey Handbook, Title 430-VI*. Retrieved 04 August 2009, from <http://soils.usda.gov/technical/handbook/>
- United States Department of Agriculture, Soil Conservation Service. (18 September 2008). *Soil Survey Manual*. Retrieved 03 August 2009, from
<http://soils.usda.gov/technical/manual/>

THIS PAGE INTENTIONALLY LEFT BLANK

INITIAL DISTRIBUTION LIST

1. Defense Technical Information Center
Ft. Belvoir, Virginia
2. Dudley Knox Library
Naval Postgraduate School
Monterey, California
3. R. C. Olsen
Naval Postgraduate School
Monterey, California
4. Marine Corps Representative
Naval Postgraduate School
Monterey, California
5. Director, Training and Education
MCCDC, Code C46
Quantico, Virginia
6. Director, Marine Corps Research Center
MCCDC, Code C40RC
Quantico, Virginia
7. Marine Corps Tactical Systems Support Activity
(Attn: Operations Officer)
Camp Pendleton, California
8. Head, Information Operations and Space Integration Branch
PLI/PP&O/HQMC
Washington, DC